

Reactive multilayer nanofilms: time of scientific and technological maturity

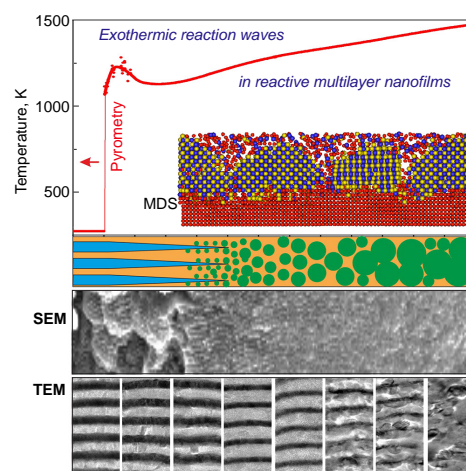
Alexander S. Rogachev^{a,b} 

^a University of Science and Technology MISIS,
Leninsky prosp. 4, stroenie 1, 119049 Moscow, Russian Federation

^b Merzhanov Institute of Structural Macrokinetics and Materials Science,
Russian Academy of Sciences (ISMAN),
ul. Akademika Osipyana 8, 142432 Chernogolovka, Moscow Region, Russian Federation

The analytical review presents the results of recent research and the latest developments in the field of reactive multilayer nanofilms (RMNFs), which were first obtained in the mid-1990s and have now formed a special class of energetic materials produced by layer-by-layer deposition. This class includes M/Al systems ($M = \text{Ni}, \text{Ti}, \text{Zr}, \text{Pt}, \text{Pd}$), other bimetallic systems (Ni/Ti , etc.), M_1/Nm systems ($M_1 = \text{Ti}, \text{Zr}, \text{Nm} = \text{Si}, \text{B}, \text{C}$) and thermite systems (Al/CuO , etc.) and continues to expand. The emergence of RMNFs stimulated elaboration of new experimental diagnostic methods and computer models for fast physicochemical processes. It is shown that the reaction in the front of a self-propagating exothermic wave occurs in a time of the order of microseconds, which is determined by the rate of dissolution of the solid reactant in the melt of the second, low-melting reactant (usually Al) and by the rate of liquid-phase diffusion. The unique properties of reaction waves in RMNFs are used in novel technologies for bonding of dissimilar materials. The bibliography includes 160 references.

Keywords: reactive multilayer nanofilms, structure, reaction mechanism, materials bonding.



Contents

1. Introduction	1	4.2. Dynamic transmission electron microscopy	6
2. Manufacture of reactive nanofilms	2	4.3. <i>In situ</i> synchrotron X-ray diffraction	8
3. Classes of reactive nanofilms in terms of chemical composition	3	4.4. Modelling of the reaction cell and reaction wave as a whole	8
3.1. Metal–metal systems	3	5. Relationship of the reaction mechanisms with combustion wave propagation patterns and practical use of thin-film SHS	10
3.2. Metal–non-metal systems	4	6. Industrial production and applications of reactive nanofilms	11
3.3. Thermite mixtures (metal oxide–aluminium)	5	7. Conclusion	12
4. Mechanisms of heterogeneous reactions in nanofilms	5	8. List of abbreviations and symbols	12
4.1. Quenching of the combustion wave and electron microscopy of the microstructure and crystal/atomic structure in the reaction zone	5	9. References	12

1. Introduction

The first patent for the manufacture of multilayer films consisting of alternating nanosized layers of reactants in which it is possible

A.S.Rogachev. Doctor of Physical and Mathematical Sciences, Chief Researcher at ISMAN, Professor of MISIS.

E-mail: rogachev@ism.ac.ru

Current research interests: dynamics of phase and structural transformations in high-temperature processes in microheterogeneous, nanoheterogeneous and amorphous systems; mechanisms of propagation of combustion waves in microheterogeneous media and nanosystems; self-propagating high-temperature synthesis of advanced materials; structure formation in reaction products under combustion and thermal explosion conditions; macrokinetics and chemical kinetics of fast processes; reaction waves in thin multilayer films; mechanical activation of heterogeneous reactions.

Translation: Z.P.Svitanko

to initiate a self-propagating wave of exothermic reaction was granted in 1996.¹ After that, the intensity of research along this line rapidly increased. Methods for the fabrication of reactive multilayer nanofilms (RMNFs) have been improved; new chemical compositions of RMNFs have been developed; the propagation of reaction waves in the films has been investigated. It was shown that exothermic reaction waves in RMNFs are due to gasless combustion, which is a type of self-propagating high-temperature synthesis (SHS). The results of the first stage of research were analyzed in our review published in 2008.² In our opinion, the key results of the first stage are as follows:

(1) the existence of gasless combustion waves (thin-film SHS) was established and the features of their propagation in M/Al ($M = \text{Ni}, \text{Ti}, \text{Co}, \text{Nb}, \text{Pt}$) and M/Si ($M = \text{Ni}, \text{Nb}, \text{Ti}$) RMNFs were determined;

(2) using the layer models of the reaction medium, it was possible to explain, although roughly (by taking abnormally

high diffusion coefficients), the observed combustion regularities and unusually high reaction wave propagation velocities;

(3) basics for the technique of joining dissimilar materials using RMNFs were developed.

Over the past years, the research area has markedly expanded. RMNFs with new chemical compositions were manufactured and studied. Among them were thermite films (*i.e.*, films consisting of metal oxide and aluminium), which showed unusual combustion modes not observed previously. New experimental and theoretical results disclosing the mechanisms of heterogeneous reactions in thin-film SHS waves were obtained. For the study of these processes, dynamic X-ray diffraction techniques were developed and utilized, using synchrotron radiation, dynamic *in situ* transmission electron microscopy (DTEM) and molecular-dynamic simulation (MDS). New results are summarized in a number of reviews^{3–8} and as separate monograph chapters devoted to thin-film SHS.^{9,10} Mention should also be made of thesis papers^{11–14} and university editions¹⁵ on this subject. Reactive nanofilms started to be manufactured on an industrial scale and used to solve numerous problems in microelectronics, aerospace engineering and other modern technologies and industries. Thus, the last 10 to 15 years of research can be characterized as a stage of scientific and technological maturity of the new research area.

The purpose of this review is to describe the general picture of the progress of this field of science and technology over the last 15 years, with attention being focused on new methods for RMNF manufacturing and study, new chemical compositions and unusual combustion modes, and both existing and potential applications.

2. Manufacture of reactive nanofilms

The key method for manufacturing RMNFs is magnetron sputter deposition from two or more magnetron sources. Most often, pure metals are used as magnetron sputtering targets (sources of the deposited atoms). Prismatic carousel holders for the substrates are used to increase the performance of the method (Fig. 1). The substrates for deposition of multilayer films are attached to faces of an octagonal prism, while magnetron sources are located on the opposite sides of the prism. As shown in Fig. 1, two opposing targets are needed to produce a Ni/Al type two-component RMNF. In order to obtain three or more alternating reactant layers, the number of sources can be increased; however, in the publications known to date, the number of sources does not exceed four.^{10,15} As the number of sources increases, it becomes the more difficult to avoid intermixing of atomic fluxes and, hence, mixing of different atoms on the substrate, which decreases the reaction heat. The

intermixing of atoms during the deposition is also reduced by cooling down the substrate and by decreasing the energy of atoms or ions colliding with the substrate. The kinetic energy of atoms during the magnetron sputter deposition can be decreased by increasing the argon pressure in the vacuum chamber to tenths of Pascals;¹⁰ however, this is accompanied by increasing mechanical stress in the deposited layers and does not completely eliminate mixing at the layer interfaces. The deposition of atoms with low kinetic energy may be accomplished by simple evaporation of metals in high vacuum; in some studies, the electron-beam evaporation of metals was used to form Ni and Al nanolayers.^{16–18} The mechanisms of mutual penetration of Ni and Al atoms at the interface between the deposited layers were modelled using the density functional theory (DFT) and kinetics of heterogeneous reactions.^{19,20} It was shown that nickel deposition onto an aluminium layer is accompanied by exothermic penetration of Ni atoms into aluminium, characterized by low activation energy. Meanwhile, when aluminium is deposited onto a layer of nickel, the diffusion of Al atoms requires overcoming a high activation barrier and is endothermic. Modelling has not yet answered the question about the minimum possible layer of mixed atoms at the interface between the reactant layers; currently, mixing is minimized empirically, most often, by efficient cooling of the substrate.

The substrates used to deposit RMNFs are, most often, polished metal sheets or foils (steel, copper, *etc.*). Owing to intense cooling, the multilayer film is not strongly bonded to the substrate and is detached as a reactive multilayer foil (RMF; below the term ‘foil’ is used to refer to metal films detached from the substrate). Examples of industrially manufactured reactive Ni/Al foils are shown in Fig. 2*a*. In some cases, the reactive foils are separated from the substrate by dissolving the substrate. For example, Zr/Al RMF was deposited onto a copper foil substrate and then copper was dissolved in aqueous HNO₃ to obtain RMF samples.¹⁵ A study of Ni/Al RMNFs deposited on substrates of various chemical compositions (AlN, AlNi₃, Si, Al₂O₃) with different surface roughnesses demonstrated that the substrate affects the shape of layers and the film reactivity.²¹ RMF sheets like those shown in Fig. 2*a* can be used to manufacture differently shaped products such as rings, ribbons, serpentes and so on by means of stamping or chemical etching¹⁰ or cutting with short laser pulses (to avoid initiation of the reaction).²²

When it is necessary to obtain reactive films in the form of micro-sized particles of different shapes, special types of substrates are used. Flake-like RMNFs were obtained by magnetron deposition of Ni/Al RMNF on nylon meshes of 50 μm in diameter with a square weave (Fig. 2*b*), which made it possible to decrease and precisely control the propagation velocity of the gasless combustion wave.²³ The combustion rate within each flake corresponded to the rate of combustion of a

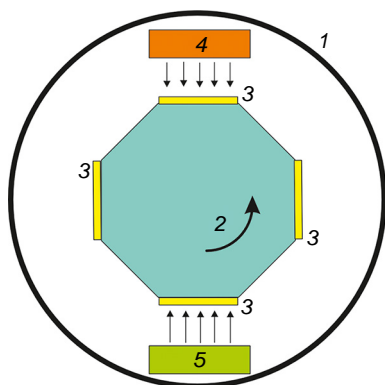


Figure 1. Design of the device for magnetron sputter deposition of RMNFs: (1) vacuum chamber, (2) cooled prismatic carousel holding the substrates, (3) substrates for RMNF deposition, (4) magnetron source for the first reactant, (5) magnetron source for the second reactant. The scheme is based on the description given in Ref. 10.

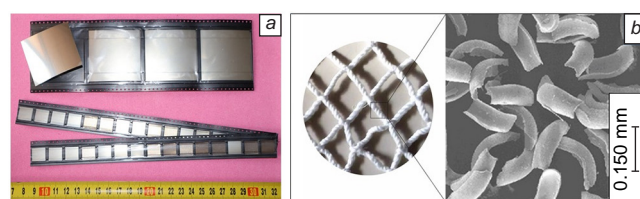


Figure 2. Reactive Ni/Al foils: (a) deposition of commercially produced foil on a smooth substrate (author's photo), (b) flake-like RMNF fabricated by deposition onto a nylon mesh (based on published data.²³).

continuous film, but at the contact between the flakes, burning was retarded; thus, the average combustion rate of a layer of these particles could be decreased to a desired value by controlling the size of flakes and, hence, the number of contacts per unit length. Electron-beam deposition on porous alumina substrates was used to fabricate reactive Ni/Al nanorods¹⁷ of 60 nm in diameter and fractal microstructures¹⁸ to be used as nano-sized local sources of heat.

Despite the attained progress, the fabrication of RMNFs by layer-by-layer magnetron sputtering and vacuum deposition are still relatively slow (the film growth rate is a few micrometres per hour) and expensive; therefore, the use of these techniques is justified only for solving critical tasks in microelectronics, precision mechanics or aerospace engineering. For wider use of reactive foils, a relevant issue is to develop high-throughput and inexpensive methods for their fabrication. A certain progress has also been attained along this line. As noted in our earlier publications,^{2,24} mechanical treatment of powder mixtures in ball mills affords multilayer particles consisting of submicron reactant layers, while cold rolling of these mechanically treated powders gives rise to reactive strips comparable in the properties with RMNFs. A significant achievement is the fabrication of Al- or Sn-coated reactive Ni/Al strips using this approach and the application of these strips for bonding aluminium and silicon parts.^{18,25} The attempts to use mechanically activated Ni/Al nanopowders without cold rolling for bonding were unsuccessful.²⁶ Despite the fact that the particle size was comparable with the layer thickness in RMNFs, the combustion velocity proved to be 2–3 orders of magnitude lower than that in reactive nanofilms deposited by magnetron sputtering.

Encouraging results were obtained when the electrochemical deposition was combined with hot pressing.²⁷ An aluminium foil with a 5.5 μm thickness, together with a 1–2 mm-thick pure nickel plate, were immersed into an aqueous electrolyte based on NiSO_4 , NiCl_2 and H_3BO_3 . An electrical current of 3 A dm^{-2} was passed between the plate and the foil; as a result, 1.8 μm -thick nickel layers were deposited on both sides of the foil. After that, the foil was cut into square pieces with a 5 mm side, which were stacked and compressed at a temperature of 673 K under compressive pressure of 280 MPa for a period from 30 min to 4 h. This gave 1–8 mm-thick monolithic samples consisting of alternating smooth aluminium and nickel layers with 8–9 μm total thickness of a bimetallic layer. Although the bilayer thickness was approximately 200 times greater than that in the sputtered RMNFs, an exothermic reaction with heat evolution of up to 1003 J g^{-1} (85.9 kJ mol^{-1}) was initiated in the obtained foils on heating to 740 K in a differential scanning calorimeter. The released heat was almost 72% of the heat of reaction $\text{Ni} + \text{Al} = \text{NiAl}$, although no self-propagating wave was yet obtained in the cited work.²⁷ The existence of self-propagating waves of exothermic reaction in electrochemically deposited Pd/Sn films was reported by Hertel *et al.*²⁸ The films were deposited on silicon substrates coated by thin gold or copper layers using two electrolytes, one to deposit a tin layer ($\text{pH} = 1-2$; Sn concentration of 20 g L^{-1}) and the other to form a palladium layer ($\text{pH} = 7-8$; Pd concentration of 8 g L^{-1}). The electrolytes were located in different baths; a soluble anode made of tin metal was immersed into a bath with a tin-based electrolyte, while a platinum-coated titanium anode was immersed into a bath with a palladium-based electrolyte. For deposition of a multilayer film, the substrate was alternately immersed into each bath, which resulted in the deposition of 30–60 bilayers. After the appropriate number of cycles, samples

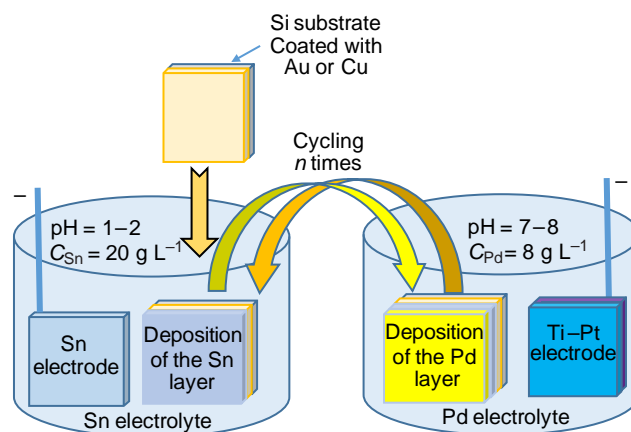


Figure 3. Diagram of the fabrication of Sn/Pd RMNFs by alternating electrochemical layer deposition in baths containing different electrolytes.

with bilayer thickness of 425 and 511 nm were formed, as illustrated in Fig. 3. The propagation velocity of the gasless combustion wave was 5.704 m s^{-1} in a 60×425 nm film and 4.478 m s^{-1} in a 30×511 nm film. Using these films, bonding of model electronic chips was performed. A drawback of this method is the necessity to repeatedly transfer the substrate from one electrolytic bath to another; however, it was reported that development of an electrolyte containing ions of both metals is in progress.^{28,29} If this research is a success, this will enable layer-by-layer deposition of the reactants in one electrolyte by merely changing the electrical voltage and current.

To conclude this Section, we will consider a recently developed original method for the fabrication of conducting structures in various microelectronic devices using RMNFs.³⁰ The Al/Zr/C multilayer films were sputtered from three magnetron targets onto polymer mesh substrates in a setup that is depicted in Fig. 1 to form flaky particles similar to those shown in Fig. 2*b*. Then the resulting powder consisting of flaky particles was mixed with a solution of cellulose in dimethylformamide and thus jet printer ink was obtained. This ink was used to print the desired structures (circuits) on substrates; after drying at 373 K, they retained 98.8 mass% of the reactive particles and 1.2 mass% of the binder. After local ignition, an exothermic reaction wave was generated in these structures, giving rise to a mechanically and thermally stable product with a good electrical conductivity. This new engineering concept was patented³¹ and called ‘reaction-assisted ink for longevity’.³⁰

3. Classes of reactive nanofilms in terms of chemical composition

As regards the chemical composition, the main classes of RMNFs that are currently at the focus of research and development are metal–aluminium, metal–non-metal (silicon, carbon, boron) and metal oxide–aluminium systems.

3.1. Metal–metal systems

Among aluminium-containing bimetallic systems, most publications are still devoted to Ni/Al RMNFs fabricated by magnetron sputter deposition. New studies are aimed at the generation of specific microstructure in these films, which

would make it possible to control the combustion and to enhance the reliability of material bonding with these RMNFs.^{32–35} In this case, the microstructure and the properties of reactive films can be changed *via* modification of the substrate surface. For example, comparison of the Ni/Al films deposited onto a flat silicon surface and onto a wave-like surface of copper foil and separated from the substrates demonstrated that the wave-like layer morphology decreases the combustion velocity by 50% without a noticeable change in the maximum combustion temperature.³⁴ The authors assumed that the surface morphology determines the RMNF texture, which affects the pattern of propagation of the reaction wave. An unusual surface microstructure of the silicon substrate consisting of thin 8–13 μm high spikes, which was named Si grass (SiG), was fabricated by the original deep reactive ion etching process.³⁵ The Ni/Al film was deposited on this surface by magnetron sputtering, which gave rise to the microstructure depicted in Fig. 4a. It was shown that parameters of the reaction wave can be controlled by varying the height and density of arrangement of the silicon spikes (grass blades). The SiG microstructure was retained after the reaction (Fig. 4b). In addition, the decrease in the heat losses into the silicon substrate owing to this microstructure made it possible to generate a self-sustained combustion wave in a very thin (5 μm -thick) layer.

The influence of the crystallographic orientation of the single-crystalline nickel substrate on the Ni/Al RMNF structure was studied by molecular dynamic simulation, which revealed the possibility of epitaxial growth of reactant layers.³⁶ Experimental study of the combustion of RMNFs on various substrates (gold, copper, silicon) confirmed the possibility of controlling the reaction wave parameters *via* heat loss to the substrate.³⁷ Recently, setups for magnetron sputtering of multilayer films were designed and manufactured for the industrial production of Ni/Al RMNFs for microelectronic applications and original methods were developed for measuring the combustion velocities and heats of reaction.^{38,39}

Among other intermetallic systems in which combustion was implemented, mention should be made of Ti/Al,^{15,40} Co/Al,⁴¹ Zr/Al,⁴² Pt/Al,^{43–45} and Sc/Ag RMNFs.⁴⁶ Despite the discovered interesting effects such as epitaxial combustion of Ti/Al

nanolayer foil (*i.e.*, combustion in which the texture and crystallographic orientation of the initial layers of reactants are retained in the product),^{2,40,47} these systems are still less studied than the Ni/Al system. The Zr/Al system is of interest for the fact that the self-propagating gasless reaction between the metals in this system initiates the self-sustained exothermic oxidation of the intermetallic compound in the air environment; this extends the heat release period by several orders of magnitude from milliseconds to seconds.^{42,48,49} A similar effect was also found for Sc/Ag RMNFs.⁴⁶ The extended period of reaction heat release is required when RMNFs are used as local heat sources. The parameters of the reaction waves in the Co/Al system are similar to those of Ni/Al films; the maximum combustion velocity of approximately 8.5 m s^{-1} was attained for the bilayer thickness of 20 nm and film thickness of 7.5 μm .⁴¹

A considerable increase in the reaction heat and the reaction front velocity was attained in the Pd/Al⁵⁰ and Ru/Al systems.⁵¹ This effect can be attributed to higher enthalpy of formation of reaction products from the elements: for example, the enthalpy of formation of PdAl from the elements is 168 kJ mol^{-1} , which is much higher than the enthalpy of formation of NiAl (117 kJ mol^{-1}), while the molar heat capacities of Pd and Ni are similar (25.8 J K mol^{-1} and 26.1 J K mol^{-1} , respectively). Even in the micrometre-thick films on a silicon substrate consisting of twenty Pd and Al layers with a 50 nm period,⁵⁰ the reaction wave propagated at a velocity of 40 to 50 m s^{-1} . High energy characteristics (combustion velocity of 10.9 m s^{-1} , temperature of 2273 K) were also inherent in Ru/Al RMNFs,⁵² although the lowest ignition temperature of these films (680 K) proved to be higher than the ignition temperature of the Ni/Al system (490 K).⁵³

Among the intermetallic systems containing no aluminium, note the multilayer Ni/Ti film reported by Adams *et al.*⁵⁴ The combustion velocity in this system is relatively low, being in the range from 0.1 to 1.4 m s^{-1} , while the reaction initiation (ignition) temperature is 573–673 K. However, the system is of interest since titanium nickelide has a shape memory effect, which can be used in so-called microelectromechanical systems.

3.2. Metal–non-metal systems

The heat released in the reactions of transition metals with non-metals, such as carbon, boron or silicon is much higher than the heat of reactions in intermetallic systems; therefore, metal–non-metal systems are promising for the development of new RMNFs. A drawback of such systems is brittleness of non-metal layers, which prevents the fabrication of flexible reactive foils. Today, silicon-containing systems have been most studied: Ti/Si^{55,56} and Fe/Si⁵⁷ films and Ti/Si/Al ternary system^{15,58} have been obtained. Studies dealing with Nb/Si⁵⁹ and Ni/Si⁶⁰ systems that we considered previously are also worth mentioning.² The Ti/Si nanofilms separated from the substrate were manufactured by deposition of layers on a copper substrate, which was then dissolved in a special copper etching chemical (CuE-3000M; the composition of the solution was not reported).⁵⁶ It was noted that the multilayer films had very high internal stresses; therefore, the greatest film thickness did not exceed 2 μm . According to one more technique for the separation of thin sputtered films from the substrates, a 100 nm-thick sacrificial KBr layer was first deposited onto the substrate and then RMNF was deposited onto this KBr layer.⁵⁵ The microstructure of the Ti/Si films was found to be less clear-cut than that of bimetallic films, and the silicon layers were amorphous. Table 1 shows, for comparison, the microstructures

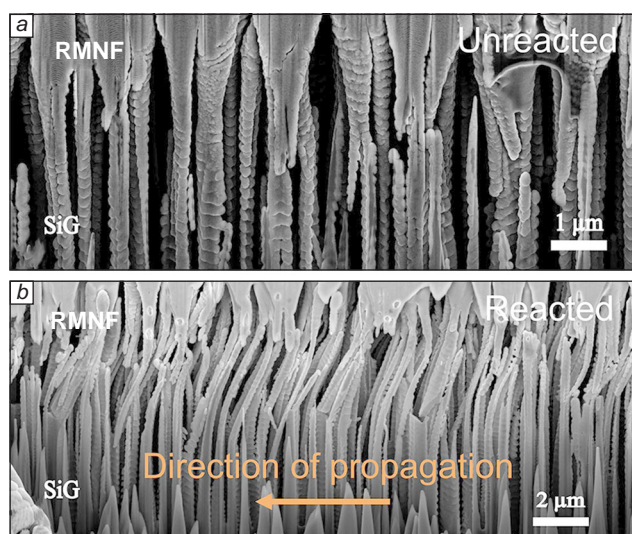
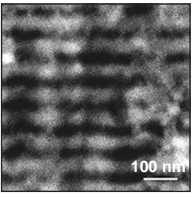
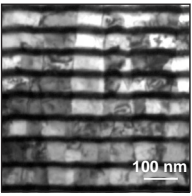
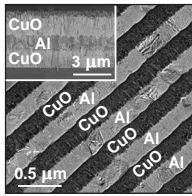


Figure 4. SEM images of the microstructure of silicon grass (SiG) with sputtered Ni/Al RMNF: (a) before and (b) after the reaction wave.³⁵

Table 1. Examples of RMNF microstructures in systems with one non-metal reactant.

RMNF	Microstructure	Comment	Ref.
5Ti/3Si		Silicon (light) and titanium (dark) layers are blurred and have an island structure. The multilayer nanostructure is poorly formed.	55
Ti/3Al		Clear horizontal interfaces between reactive layers; vertical grain boundaries are seen in the aluminium layers (light). The film consists of vertical columnar multilayer crystalline grains, which altogether form a layered polycrystalline microstructure.	55
CuO/Al		The layered microstructure is well formed, the layers are even, but a finer inhomogeneous microstructure is observed within the layers (see the inset). It can be seen that each layer is composed of smaller grains.	64

of 5Ti/3Si and Ti/3Al RMNFs (the numerals indicate the molar ratios of reactants) deposited by magnetron sputtering in the same study.⁵⁵ The thickness of the deposited films was 1–3 μm for silicon-containing films and 6–16 μm for aluminium-containing films. It was shown that 5Ti/3Si films can burn directly on the silicon substrate when their thickness is less than 2 μm , *i.e.*, less than 27 bilayers (in some cases, the substrate was heated to 573 K), which is much smaller than the minimum thickness required for Ni/Al and Ti/Al films under similar conditions. For Ti/Si/Al ternary films with bilayer thickness of 28–29 nm and the total thickness of 5.7–5.8 μm , the reaction propagation velocity was 9 m s⁻¹, with the highest temperature reaching 2050 K.⁵⁸ Thus, owing to the great amount of heat released upon the reaction of titanium with silicon, it is possible to fabricate fairly thin RMNFs with relatively small numbers of layers that would be not inferior in thermal properties to bimetallic systems in which the number of layers is an order of magnitude greater.

The reactions of transition metals (Ti, Zr, Hf, *etc.*) with carbon and boron can provide the most pronounced heat evolution among all gasless syntheses from elements. Quite recently, up to 10 μm -thick ternary Al/Zr/C RMNFs with alternating Al (29, 43 or 58nm), Zr (24 nm) and C (8 nm) layers were obtained; the phase formation during the reaction in a nanocalorimeter was studied.⁶¹ Data on the velocities and temperatures of combustion in these films are still missing.

3.3. Thermite mixtures (metal oxide–aluminium)

Thermite systems are promising because of the exceptionally high heat release; however, multilayer films with oxide layers are inferior to bimetallic foils in the mechanical properties, while combustion of thermite compositions is accompanied by noticeable gas formation and product dispersion and scattering.

These films are deposited, similarly to other types of films, by layer-by-layer magnetron sputtering (see Section 2), but brittleness of oxide layers prevents film separation from the substrate; hence, most experimental studies of the combustion of these RMNFs were carried out directly on the substrate. The best studied thermite RMNF is now the CuO/Al system, which was first obtained back in 2003.^{62,63} The reaction heat release in this system determined by differential thermal analysis is $3.9 \pm 0.9 \text{ kJ g}^{-1}$.⁶² This is much greater than the heat released in the Ni/Al system (the enthalpy of formation of NiAl from the elements is 1.4 kJ g⁻¹) or the 5Ti/3Si system (1.8 kJ g⁻¹). In view of the above-noted features of this composition, CuO/Al RMNFs are developed to be used in pyrotechnics as ignition mixtures and in triggering devices (actuators),^{64–67} in chemical micro sources of heat,^{68–70} in self-destructing microchips⁷¹ and microchips for fast (less than 100 μs) circuit break.⁷² CuO/Al films for bonding of materials were also developed.^{73,74} The microstructure of thermite RMNF is composed of smooth and clearly separated layers, as shown in Table 1.⁶⁴

The vigorous gas evolution that usually accompanies the combustion of thermite compositions is not always desirable, since it gives rise to pores and results in dispersion of condensed products (*i.e.*, scattering of the products as particles and drops). These effects must be avoided, *e.g.*, when RMNFs are used for material bonding. In order to suppress gas release, less energetic Cu₂O/Al mixtures were used, with copper metal layers being incorporated into the multilayer film structure (Cu₂O/Al/Cu) to serve as an inert diluent.^{75,76} Using this approach, it was found that vaporization of copper can be suppressed if the copper content in the foil is approximately 40 mass%.⁷⁶

It is of interest that despite the very great heat release of the reaction in the CuO/Al RMNF, the temperature of initiation of the self-sustained reaction in this system proved to be relatively high— $1150 \pm 100 \text{ K}$.⁷⁷ The ignition delay time can be reduced to $59 \pm 3 \mu\text{s}$ by decreasing the thickness of the reactive layers and increasing the local area of heating. Some characteristic features of initiation of nanothermites were summarized in a review.⁷⁸

4. Mechanisms of heterogeneous reactions in nanofilms

4.1. Quenching of the combustion wave and electron microscopy of the microstructure and crystal/atomic structure in the reaction zone

Quenching of the combustion wave is a common method for studying the mechanisms of SHS reactions.⁹ The essence of the method is that the reacting sample is placed under conditions of large heat losses that increase as the combustion wave moves on and lead, at some point, to combustion extinguishing and rapid cooling (quenching) of the intermediate and final products at different points of the sample. For example, a mixture of powdered reactants is pressed into a wedge-shaped cut-out in a bulk copper block, and the reaction is initiated at the wide side of the cut (at the base of the wedge). As the combustion front moves towards the narrow part of the wedge, specific heat losses increase, and the combustion front stops before reaching the top of the wedge-shaped cut-out. Then the evolution of the phase composition, microstructure and crystal structure is studied along the wedge-shaped sample taken out of the cooling block from the narrow side to the wide one, in order to reconstruct the picture of transformation of the initial reaction mixture (in the narrow part of the wedge) into the final product (in the wide part).

A similar approach was used to study the mechanism of gasless combustion of Ni/Al RMNF in a series of works.^{79–81} The results of high-speed video and micropyrometry showed that combustion is a two-stage process (Fig. 5a). The first stage lasts for approximately 0.5 ms and is characterized by a very rapid temperature rise (the heating rate at the front of the reaction wave is up to a million Celsius degrees per second). This is followed by a slower second stage, which lasts for a few tens of milliseconds, and the temperature rise at this stage does not exceed 30–40 thousand degrees per second. In view of the small thickness of reactive foils, they could hardly be cut into a wedge. Therefore, to quench the combustion wave, constant-thickness foils were clamped between two copper blocks in such a way that some of the foil freely protruded outward (Fig. 5b). The combustion was initiated in the free part of the foil and extinguished in the gap between the cooling blocks. For quenching of the reaction wave, the rate of heat sinking into copper should compete with the rate of reaction heat release. Since the exothermic reaction in Ni/Al RMNF is very fast, quenching is possible only for a foil that is less than 20 μm thick and is strongly pressed to the polished copper surface to enhance

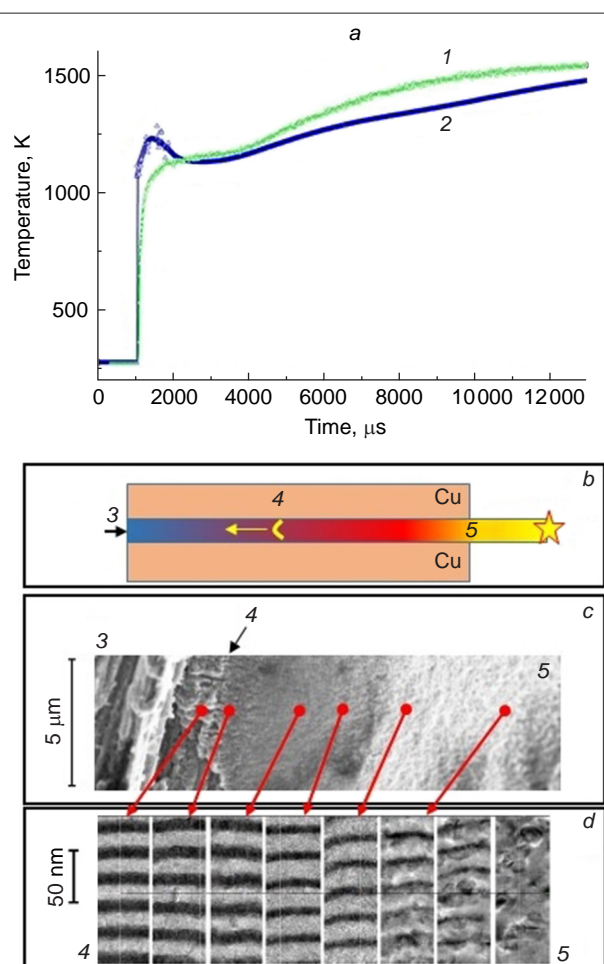


Figure 5. (a) Temperature profiles of the combustion of Ni/Al RMNF derived from high-speed video footage (1) and measured with a micropyrometer (2); (b) quenching of the gasless combustion wave in RMNF; (3) initial RMNF, (4) reaction zone, (5) product; (c) SEM image of a sample fracture with the quenched reaction front; (d) scanning transmission electron microscopic image of local sites at different distances from the quenched front (dark nickel layer). (the plots and photographs were taken from the author's archive to Ref. 79.)

the thermal contact. When the heat loss is intense, the second stage never starts, and the reaction wave propagates as a thin luminous band only due to the first reaction stage. Both the first and second stages of the reaction give nickel monoaluminide NiAl, as shown by powder X-ray diffraction, electron microscopy (Fig. 5c,d) and energy dispersive X-ray spectroscopy. The intermediate intermetallic compounds such as Ni₂Al₉, which were observed previously in Ni/3Al films upon slower heating,⁸² are not formed in this case. Detailed examination of the reaction zone by transmission scanning electron microscopy and microanalysis (Fig. 5d) showed that the first stage of the reaction comprises melting of aluminium layers and dissolution of nickel in the melt without the formation of solid products. The second, slower stage corresponds to the continuing heterogeneous reaction to give NiAl grains at the interface between the layers. However, it was shown that the grains of the solid product do not coalesce into a continuous layer separating the reactants; therefore, nickel atoms can continue entering the melt through gaps between the grains. The absence of a continuous layer of the solid product accounts for the high propagation velocities of the reaction wave.

A fairly unusual combustion mechanism was detected for CuO/Al RMNF.⁸³ This film consisted of 20 bilayers of the reactants and had a total thickness of 2 μm , and the reaction was initiated in the film deposited on a single-crystalline silicon substrate. High-speed macro video recording was carried out, and the microstructures of quenched combustion waves were investigated. It was shown that the reaction product forms drops with a size of a few to a few tens of micrometres consisting of two immiscible melts, copper-based metallic melt and Al₂O₃ oxide melt. Under the action of surface tension forces, these drops move at a velocity of approximately 6 m s^{-1} , together with the reaction wave front as if riding over this front. Therefore, this mechanism was called a riding combustion mode.⁸³ A schematic view of this RMNF combustion mode and microstructure of the reaction zone are sketched in Fig. 6.

Later, the effect of the layer thickness on the combustion and on the products was investigated.^{84,85} The following issues are worth mentioning: when the combustion arrives to the edge of the substrate, the product drops, which continue to move by inertia, are separated from the substrate and flow in a direction determined by the propagation direction of the combustion front at a velocity of 5–6 m s^{-1} . This can be used to develop triggering devices (microactuators).

4.2. Dynamic transmission electron microscopy

The combustion wave quenching techniques provide only indirect information on the microstructure of the reaction zone, since the composition of the heterogeneous medium that reacts at high temperature is derived from material that has already cooled down and crystallized. Therefore, it would be quite useful to obtain an electron microscopic image of a 'living' combustion wave *in situ*, that is, directly during a high-temperature reaction. This problem seems unsolvable, in view of the instantaneous time (ranging from microseconds to milliseconds) and high temperature of the reaction. Nevertheless, this task was set and partially solved.^{86,87} A lump of 3 Ni/2 Al RMNF with a total thickness of 125 nm consisting of five bilayers was placed into the column of a transmission electron microscope. A snapshot of the combustion process was obtained using the photocathode of the microscope. On irradiation with a short laser pulse (15 ns at 211 nm), the cathode ejected a bunch of electrons a few orders of magnitude more intense than the

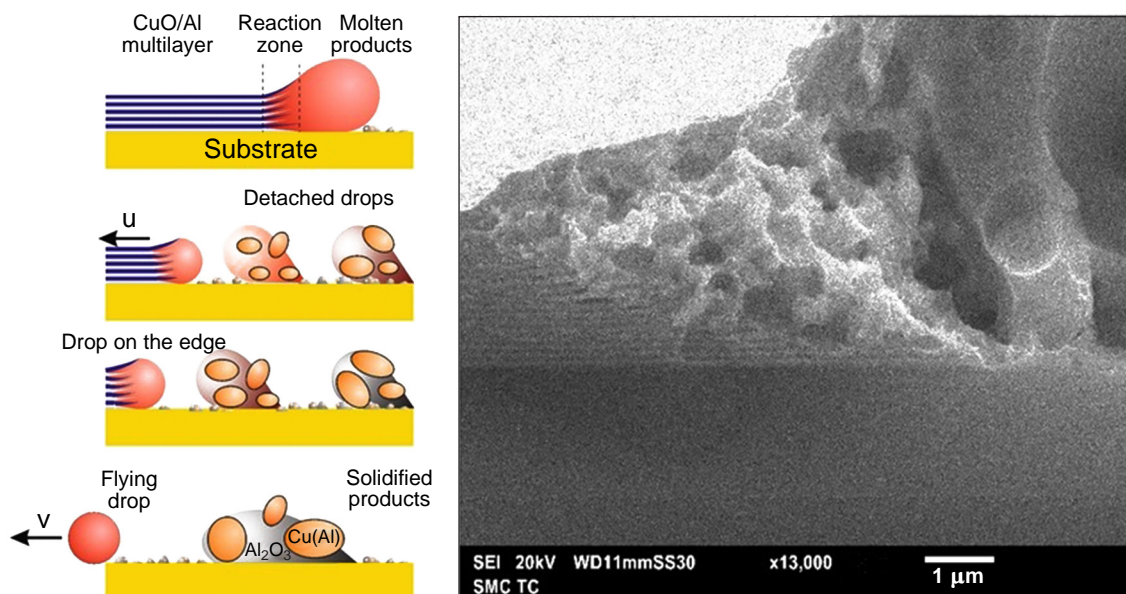


Figure 6. Schematic view of the riding combustion mode of CuO/Al RMNF (a) and SEM image of the microstructure of the reaction zone near the combustion wave front (b). The character u stands for the linear velocity of the combustion wave, v is the velocity of the product drops after detachment from the substrate (taken from the author's archive to Ref. 83).

electron beam in the usual operation mode of the microscope. The reaction in the foil was initiated by a 3 ns infrared laser pulse at a wavelength of 1064 nm, which was synchronized with the pulse of the first laser. The transmitted electron image was detected by a charge-coupled device (CCD detector).^{41,88,89} This procedure, which is sketched in Fig. 7, was called dynamic transmission electron microscopy (DTEM), further developed and used to study the mechanisms of fast chemical reactions and structural phase transitions,^{90,91} in particular in combination with nanocalorimetry.⁹² Instead of a single pulse, a series of short pulses started to be used for irradiation of the photocathode, which gave rise to a sequence of snapshots for the dynamic process. Figure 7 shows an example of such a sequence for the combustion of 2Ti/3B RMNF.⁹⁰ The results of application of DTEM for studying the dynamics of chemical processes on a nano-scale are summarized in a recent review.⁹³

As noted above, DTEM only partially solves the problem of *in situ* monitoring of fast RMNF combustion. As can be seen in Fig. 7, all images were obtained by illuminating the sample perpendicular to its surface, and the interaction between the reactant layers can be observed only in the cross-section of the film, as shown in Fig. 5. More information about the chemical reaction dynamics can be gained from the sequence of electron microdiffraction patterns, which were also obtained by DTEM.^{86,90} According to the results, NiAl is formed just behind the combustion wave front in 3Ni/2Al film,^{86,89} while in the case of 2Ti/3B film, TiB_2 grains are formed.⁹⁰ In other words, the most high-melting phase present in the system is the first to crystallize upon the reaction.

The dynamics of the product formation was studied *in situ* for a large group of various thin-film structures using electron micro-diffraction. The samples were slowly heated (at a rate of a few degrees per minute) directly in a transmission electron microscope; the electron micro-diffraction patterns were supplemented by the results of electron microscopy, thermal analysis and electrical and magnetic measurements. Currently, data on the following nanolayered films are available: Fe/Al,⁹⁴ Cu/Al,^{95–97} Pt/Al,⁹⁸ Pt/Co,^{99,100} Fe/Pd,^{101,102} Fe/Rh,^{103,104} Sc/Ag,⁴⁶ Cu/Sn,¹⁰⁵ Ag/Al,¹⁰⁶ Cu/Si,¹⁰⁷ Al/Si,¹⁰⁸ In/Co₃O₄,¹⁰⁹

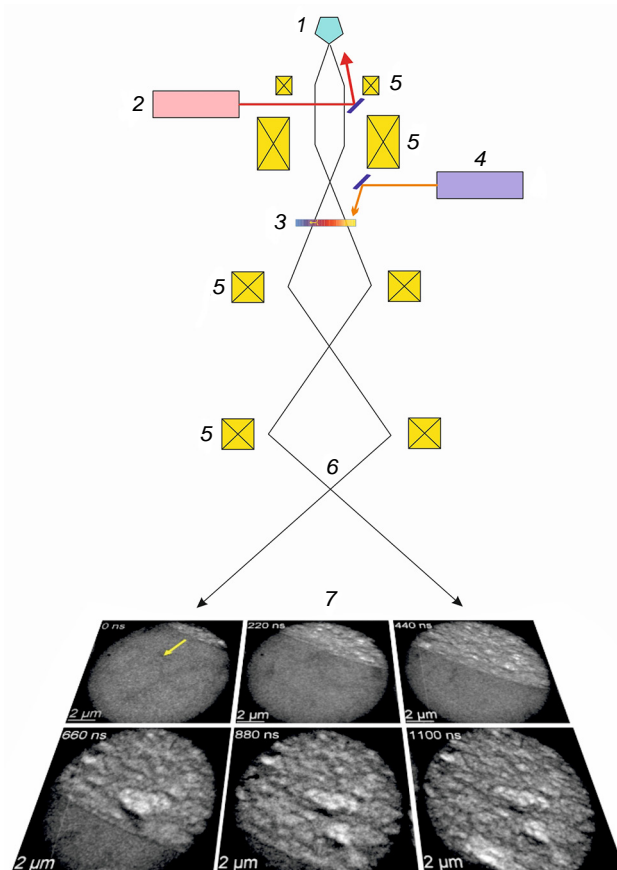


Figure 7. Design of the dynamic transmission electron microscopy: (1) photocathode; (2) laser for the control of the photocathode (15–17 ns pulse duration); (3) RMNF sample in which the reaction wave propagates; (4) laser that ignites the sample (initiates the reaction at the initial point; 3 ns pulse duration); (5) electron lenses; (6) electron beam; (7) images detected by a high-speed CCD camera (the images were adapted from Ref. 90).

Zr/Co₃O₄ (Ref. 110) and Fe/Co₃O₄.¹¹¹ Although self-sustained reaction waves (combustion waves) have not yet been implemented in these structures, the obtained results provide extensive experimental material for understanding of the reaction mechanisms in nanolayered systems and for the development of new chemical compositions of RMNFs. Using slow cooling with simultaneous *in situ* monitoring of structural transformations, one can identify all possible stages of structure formation in the reaction products; however, only RMNF combustion experiments make it possible to decide which of these stages actually take place during the combustion.

4.3. *In situ* synchrotron X-ray diffraction

Single crystal and powder X-ray diffraction are the key methods for precise determination of phase crystal structures in materials. However, investigation of fast chemical structural transformations in RMNFs requires a very high radiation intensity, which can be attained only in synchrotron sources. Therefore, all results known to date were obtained at various synchrotron stations. The Cornell High Energy Synchrotron Source was used to investigate 30 μm-thick Ni/Al foils consisting of alternating Al (70 nm thick) and Ni (30 nm thick) layers.¹¹² The synchrotron radiation was focused onto a spot of 60 μm in diameter on the RMNF surface, while an extremely fast pixel array detector was located on the opposite side of the foil, *i.e.*, the diffraction patterns were taken in transmission. The recording was triggered by the signal of a photodiode, which received radiation from the combustion wave. As a result, up to eight successive diffraction patterns could be collected in a single experiment, each being formed within 55 μs. It was shown that the cubic NiAl phase is the first product formed just behind the reaction front. Ni/Al RMNFs composed of thinner layers (bilayer thickness of 40 nm) were studied at the Swiss Light Source at Paul Scherrer Institute.¹¹³ The time of measurement of each diffraction pattern was relatively long, 0.125 ms. Simultaneously with synchrotron X-ray diffraction, combustion was monitored by high-speed video camera and infrared imager. The results confirmed that nickel monoaluminide was the first product phase formed in the reaction wave front.

The *in situ* synchrotron X-ray diffraction was also utilized to study the growth of oxide film that begins to form behind a gasless combustion wave in Zr/Al RMNF in air atmosphere.⁴² As noted above (Section 3.1), oxidation of intermetallic products formed in the gasless reaction wave extends the period of chemical heat release, which is required for some applications.

Interesting results were recently obtained in a study of ternary Al/Zr/C RMNF by coupling *in situ* synchrotron X-ray diffraction with nanocalorimetry.⁶¹ The nanocalorimeter provided heating of RMNF at a specified rate; depending on the heating rate, the time of measurement of a single X-ray diffraction pattern was specified in the range from 50 μs to 1 s. In the case of relatively slow heating, the reaction gave the Al₃Zr₃C₅ ternary phase; however, when the heating rate exceeded 20 °C per second, the ZrC phase formed without any intermediate phases. In the SHS mode, the reaction gave the cermet ZrC+Al, which retained phase composition after fast cooling (quenching in water), or was converted into a mixture of two phases, Al₃Zr₃C₅+Al₃Zr, when heated in a furnace and then slowly cooled together with the furnace. Thus, it was shown that products of the desired composition can be obtained by varying the heating and cooling rates.

A study dealing with imaging of the material bonding with Ni/Al RMNF stands somewhat apart from the above synchrotron

experiments.¹¹⁴ We consider this study in this Section because it also uses synchrotron radiation. Unlike diffraction experiments in which monochromatic radiation at a given wavelength was used, in this study, Ramachandran *et al.*¹¹⁴ employed so-called polychromatic, or ‘white’ synchrotron radiation, which includes all wavelengths and, therefore, its intensity is several orders of magnitude higher than that of monochromatic radiation. Hence, the radiation could pass through a sandwich composed of a silicon wafer, RMNF with a solder layer and an aluminium substrate (the total thickness was approximately 1 mm) rather than through a single foil. The synchrotron radiation that passed through the sandwich generated a shadow image (resembling a medical X-ray image) on a scintillation screen located at a 50 cm distance from the sample. This image was registered by a high-speed video camera with a spatial resolution of 2.75 μm and a speed of up to 3745 frames per second (exposure time for one frame was 0.24 ms). The relatively long exposure time precluded observation of a clear image of the combustion front, which propagated at a velocity of 4.21 m s⁻¹ and, hence, moved by approximately 1 mm during the registration of one frame. However, this technique revealed the details of solder reflow and crack and gas bubble formation during bonding of Si and Al with RMNF.¹¹⁴

4.4. Modelling of the reaction cell and reaction wave as a whole

As noted in our previous review,² the first mathematical models for the combustion of RMNFs were actually reduced to extrapolation of the standard Khaikin–Merzhanov–Armstrong layer combustion model^{9,115} to the nano-scale region. This model implies the formation of a continuous layer of the solid product at the interface between the reactant layers and occurrence of the reaction as a result of diffusion of reactant atoms through this layer. The combustion propagates along the layers, while the reactant diffusion occurs across the layers; a separate differential equation is written for each of these processes, that is, heat conduction and diffusion, respectively. The rate of diffusion mass transfer is determined by the product of the reactant concentration gradient by the diffusion coefficient, which depends on temperature according to the following relation:

$$D(T) = D_0 \exp\left(-\frac{E_a}{RT}\right) \quad (1)$$

where D_0 is the pre-exponential factor, E_a is the activation energy for diffusion, T is temperature, R is the gas constant. Most often, the diffusion coefficients are three to four orders of magnitude lower for the bulk diffusion in crystals than for the diffusion in melts (at the same temperature). Since the diffusion in solids is slow, in order to explain the high velocities of the reaction wave propagation, it was necessary to substitute greater diffusion coefficients into the mathematical model. This approach is still utilized and, according to some authors, it provides good agreement with experimental results for Ni/Al,^{116,117} Co/Al,⁴¹ Ru/Al⁵¹ and Pt/Al⁴² RMNFs. The diffusion parameters that were used for calculations are summarized in Table 2.

As can be seen from the Table, the diffusion coefficient at the adiabatic combustion temperature is in the range of $(1.5-72) \times 10^{-10} \text{ m}^2 \text{ s}^{-1}$ for all three systems. These values appear too large for the bulk solid-phase diffusion, but they are nevertheless used in the layer models. For example, the D_0 and E_a values for Ni/Al RMNF,¹¹⁶ which were criticized in our

Table 2. Reaction diffusion parameters used in the layer model.

RMNF	D_0 , $\text{m}^2 \text{s}^{-1}$	E_a , kJ mol^{-1}	Adiabatic temperature T_{ad} , K	$D(T_{\text{ad}})$, $\text{m}^2 \text{s}^{-1}$ — calculated by relation (1) ^a	Ref.
Ni/Al	2.18×10^{-6}	137	1911	3.92×10^{-10}	116
Co/Al	1.38×10^{-7}	108	1901	1.49×10^{-10}	41
Ru/Al	1.91×10^{-7}	105	2247	6.92×10^{-10}	51
Pt/Al	2.3×10^{-7}	71.94	2500	7.2×10^{-9}	42

^a The calculation was performed by the author for adiabatic combustion temperatures T_{ad} using the D_0 and E_a values reported in the indicated references.

previous review,² were recently employed for a fairly detailed simulation of the combustion wave structure.¹¹⁷ There are few data on the diffusion coefficients at a temperature equal to the combustion temperature that are obtained from independent experiments. For the 1200–1900 K temperature range, experimental data are available on the diffusion of Ni atoms in liquid Al¹¹⁸ and in NiAl¹¹⁹ and Ni₃Al melts.¹²⁰ The diffusion coefficients found for melts are $(2.0–7.0) \times 10^{-9} \text{ m}^2 \text{ s}^{-1}$,¹²¹ *i.e.*, they are only an order of magnitude greater than the solid-phase diffusion coefficients used in the layer model. Direct measurements of the solid-phase diffusion coefficient in the Ni–Al system performed by heating bimetallic samples in the column of a transmission electron microscope with simultaneous measurement of element distribution gave $D \approx 10^{-19}–10^{-16} \text{ m}^2 \text{ s}^{-1}$ for the temperature range of 623–723 K.¹²² The D values of about $10^{-9} \text{ m}^2 \text{ s}^{-1}$ were obtained only for the dissolution of nickel in liquid aluminium.¹²³ A similar diffusion coefficient for Ni in liquid Al, $7.6 \times 10^{-9} \text{ m}^2 \text{ s}^{-1}$ at 1250 K, was found by molecular dynamic simulation.¹²⁴ It cannot be ruled out, however, that the abnormally high diffusion mobility of Ni atoms in the solid product, which approaches the mobility of atoms in liquids, is caused by the relatively fast diffusion along the grain boundaries; this assumption was made in some studies.^{51, 120}

The layer model for the reaction diffusion was taken in some publications for CuO/Al RMNF to consider the conditions of precipitation,¹²⁵ heating,¹²⁶ ignition¹²⁷ and combustion.¹²⁸ It is assumed, for example, that on heating, CuO at the interface between the reactants decomposes into Cu₂O and oxygen, which reacts with Al, thus building up the Al₂O₃ layer and inducing ignition.¹²⁷ Thus, the exothermic reaction occurs *via* diffusion of O atoms through the Cu₂O + Al₂O₃ double layer of the products.

The assumption that the reaction rate is limited by diffusion through the product layers appears reasonable for the low-temperature region. However, at high temperatures, where all metal and nonmetal layers melt and decompose and some of them are intensely gasified, the reaction diffusion layer model is hardly applicable. Melting of aluminium and switching-on of the liquid-phase diffusion, which is 3–4 orders of magnitude faster than diffusion in crystals, may destroy the assumptions about the formation of continuous layers of the solid product separating the reactants and the crucial role of solid-phase diffusion.

The use of molecular dynamic simulation (MDS) has been a new approach to the theoretical investigation of the heterogeneous reaction and combustion mechanisms in RMNFs. Unlike the layer model, MDS does not require any *a priori* assumptions about the microstructure of the medium during the reaction. The microstructure, including the shape, size and the phase and chemical compositions of the products, is generated by computer calculations. However, to obtain adequate simulation results, it is necessary to correctly specify the interaction potentials

between atoms. Currently, potentials for the Ni–Al system have been studied most comprehensively;¹²⁹ therefore, original works on this subject address particularly this system.^{80, 81, 130–132} Some simulation results are shown in Fig. 8.⁸⁰ The model reaction cell included 316602 atoms (70200 Al + 246402 Ni) and represented an aluminium layer between two nickel layers; the Figure shows the cross-sections of the cell at different stages of the reaction. In the first stage (Fig. 8a), nickel is dissolved in aluminium melt without forming a solid product. In the second stage (Fig. 8b), crystalline NiAl grains are formed along the reactant boundary; however, each grain exists as a single entity, and they do not form a continuous intermediate layer. As can be seen from Fig. 8c, there are spaces between grains; therefore, nickel atoms continue to get into the melt through these spaces. It was shown that the solid product is formed only *via* dissolution of Ni in the melt with subsequent deposition of new NiAl crystal cells on the grain surface. Diffusion of Ni atoms through the crystalline grain does not play a significant role in this process. Similar results were obtained recently for the Ni/Ag multilayer system.¹³³

The molecular dynamic simulation results are analyzed and compared with experimental data in brief reviews.^{7, 134} Transition from MDS of the reaction cell to simulation of the reaction wave propagation should be recognized as a substantial progress of this simulation method attained in recent years.^{135–138} Lengthy

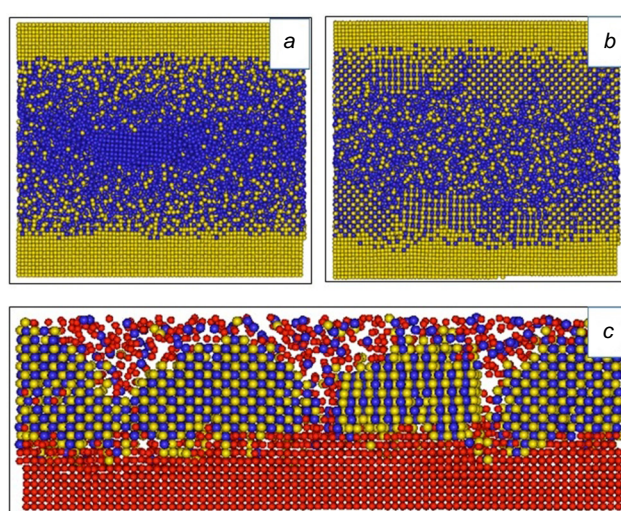


Figure 8. Molecular dynamic simulation of the reaction in Ni/Al RMNF:⁸⁰ (a) cross-section of the reaction cell in 5 ns and (b) 10 ns after onset of the reaction; Ni atoms are shown in yellow and Al atoms are blue. Structure of the product near the interface after 20 ns (c): Ni and Al atoms in the crystal structure of nickel monoaluminide are shown in yellow and blue, respectively (B2 cubic); atoms in other crystal structures or in the melt are shown in red.

films consisting of only a few reaction layers were considered. Initiation of the reaction on one side of the film results in propagation of the reaction wave along the layers in the virtual computer space, with the parameters and patterns of propagation of this wave being well correlated with experimental data.

The molecular modelling methods based on solution of a system of differential equations for diffusion (continuum model) and on molecular dynamic simulation were compared for Ni/Al RMNF.¹³⁹ It was shown that the continuum model well describes the mutual diffusion of reactants in the aluminium-based melt layer, while MDS shows all microscopic mechanisms underlying the complex mechanism of mixing of reactant atoms.

To summarize the results of Section 4, it can be stated that, according to experimental and theoretical data, the reaction wave in RMNF has a very sharp front, the reaction zone is a few micrometres wide, and the time of formation of the crystalline product is of the order of microseconds. These extreme characteristics are attained owing to fast atom transfer. The most probable mechanism of transfer is diffusion in the melt; however, some contribution of diffusion along grain boundaries to the reaction mass transfer cannot be ruled out either.

5. Relationship of the reaction mechanisms with combustion wave propagation patterns and practical use of thin-film SHS

Today, the major application of RMNFs is joining of different materials in which the reactive film is clamped between parts to be joined, the reaction in the film is initiated, the heat released upon gasless combustion induces melting of the thin layer of solder on the film surface, and thus bonding takes place. This scheme, described in many sources,^{2,8–10} resembles the scheme of combustion wave quenching shown in Fig. 5b. However, the purpose of quenching is to terminate the combustion and quickly cool the reaction products, whereas bonding of materials has the opposite objective: the reaction must occur throughout the whole RMNF, and the heat released must be sufficient for heating up the thin layer in the materials to be joined in order to ensure good wetting and solder reflow. If the reactive film is thin and heat transfer to the materials being bonded is efficient, the combustion is impossible. The smallest thickness of the combustible layer in which the combustion wave can still propagate at a specified heat loss is called the critical thickness. The problem of the combustion limit of a thermally thin layer of condensed matter (*i.e.*, a layer in which the temperature distribution across the thickness is insignificant) under heat exchange with an inert medium was solved by Rybanin and Sobolev.¹⁴⁰ The obtained results can be used to estimate the critical thickness of RMNFs. The expression for the critical thickness (d) of a planar thin layer of a burning material sandwiched between two thick inert layers has the form:¹⁴⁰

$$d = \frac{E(T_{\text{ad}} - T_0)ea_f}{RT_{\text{ad}}^2u} \sqrt{\frac{\lambda_i \rho_i c_i}{\lambda_f \rho_f c_f}} \quad (2)$$

where E is the activation energy for the combustion, which in our case coincides with the activation energy for the diffusion, since this process is diffusion-controlled; T_{ad} is the adiabatic combustion temperature; T_0 is the initial temperature of the reactive and inert layers; λ , ρ and c are the thermal conductivity, density and specific heat capacity, respectively (the subscript i refers to inert substance and f refers to the reactive foil); $e = 2.71$ is the natural logarithm base; R is the gas constant; u is the linear

velocity of combustion wave propagation; $a_f = \lambda_f \rho_f c_f$ is the temperature conductivity of the reactive layer.

The critical thickness of Ni/Al RMNF with equal molar amounts of Ni and Al can be roughly calculated as follows. The thermal conductivity of such a multilayer foil in the perpendicular direction to the layers, calculated using the law of summation of thermal resistances,¹⁴¹ amounts to $\lambda_f = 120.4 \text{ W m}^{-1} \text{ K}^{-1}$. This exceeds the thermal conductivity of Ni ($90.9 \text{ W m}^{-1} \text{ K}^{-1}$), but is lower than that of Al ($237 \text{ W m}^{-1} \text{ K}^{-1}$). Using the additivity property of the specific volumes and heat capacities, it is easy to find that $\rho_f = 5165 \text{ kg m}^{-3}$ and $c_f = 588 \text{ J kg}^{-1} \text{ K}^{-1}$. The adiabatic temperature of combustion of the Ni + Al mixture is $T_{\text{ad}} = 1911 \text{ K}$, and the initial temperature is $T_0 = 300 \text{ K}$. By substituting these values into relation (2), one gets

$$d = 2.98 \times 10^{-13} \frac{E \sqrt{\lambda_i \rho_i c_i}}{u} \quad (3)$$

Here all quantities are expressed in SI units and the critical thickness is in metres. As can be seen from the relation, when the thermal parameters of RMNFs are set, the critical thickness of the reactive foil depends on the activation energy for the combustion, reaction propagation velocity and the thermal activity ($\lambda_i \rho_i c_i$) of the inert materials meant for bonding.

The most uncertain value here is the activation energy E . In the layer model considered above, it was taken that $E = 137 \text{ kJ mol}^{-1}$ (see Table 2). However, this value was not found in independent experiments, but was determined on the basis of measured combustion velocity; it is too low for a solid-phase bulk diffusion, but too high for the diffusion in an aluminium melt. For example, the diffusion of aluminium atoms in nickel has an activation energy of 268 kJ mol^{-1} (at temperatures of up to 1600 K).¹⁴² A direct measurement of the activation energy for Ni diffusion in the NiAl intermetallic compound performed by the radioisotope method at temperatures up to 1630 K gave $E = 3.0 \pm 0.07 \text{ eV} = 289 \pm 7 \text{ kJ mol}^{-1}$.¹⁴³ Molecular dynamic simulation of the diffusion of Ni and Al atoms in NiAl showed that Al diffusion is 2.5 times slower than Ni diffusion;¹⁴⁴ hence, the activation energy for aluminium atoms can be expected to be even higher. On the other hand, diffusion in melts has a very low activation energy. The MDS method gave $E = 0.38 \text{ eV} = 36.6 \text{ kJ mol}^{-1}$ for Ni diffusion in the $\text{Al}_{0.875}\text{Ni}_{0.125}$ melt; this value gradually increases with increasing nickel concentration in the melt to reach a value of $0.60 \text{ eV} = 57.8 \text{ kJ mol}^{-1}$ for a pure nickel melt.¹⁴⁵ The diffusion of Al atoms is characterized by $E = 0.31 \text{ eV} = 29.9 \text{ kJ mol}^{-1}$ in a pure aluminium melt and $0.69 \text{ eV} = 66.5 \text{ kJ mol}^{-1}$ in a melt containing excess nickel, $\text{Al}_{0.125}\text{Ni}_{0.875}$. Finally, experimental measurement of the self-diffusion coefficients in aluminium melt by quasi-elastic neutron scattering gave $E = 0.274 \text{ eV} = 26.4 \text{ kJ mol}^{-1}$ for temperatures of up to 1193 K (Ref. 146) and $E = 0.28 \pm 0.07 \text{ eV} = 27 \pm 7 \text{ kJ mol}^{-1}$ for temperatures below 1060 K .¹⁴⁷ Thus, depending on the reaction mechanism, the E value in relations (2) and (3) can change by an order of magnitude from 26 kJ mol^{-1} (if direct dissolution and diffusion in the melt are the rate-limiting stages) to 289 kJ mol^{-1} (if the reaction is rate-limited by the reactant diffusion through the layer of solid NiAl). The results of calculations by relation (3) performed for various activation energies and various inert materials are summarized in Table 3. The combustion velocity was taken to be 10 m s^{-1} , which is typical of Ni/Al RMNF with a bilayer thickness of $20\text{--}25 \text{ nm}$.²

The results of rough calculations clearly demonstrate that the assumption of the rate-limiting role of bulk diffusion through the crystalline product layer leads to too large d values. The

Table 3. Calculation of the critical thickness of Ni/Al RMNF by formula (3).

Characteristics of inert materials to be bonded				Critical foil thickness, d , μm (depending on the activation energy E , kJ mol^{-1})		
chemical composition	λ_p , $\text{W m}^{-1} \text{K}^{-1}$	ρ_p , kg m^{-3}	c_p , $\text{J kg}^{-1} \text{K}^{-1}$	$E = 289$	$E = 137$	$E = 26$
Cu–Cu	401	8920	384.6	320	152	29
Si–Si	149	2330	718	138	65	12
Ti–Ti	21.9	4540	524	62	29	6

thickness of Ni/Al RMNFs that are actually used for bonding of material is in the range of 40–80 μm . Hence, if the reaction followed the reaction diffusion mechanism, combustion would be impossible. The average E value commonly used in layer models with allowance for the diffusion at grain boundaries also leads to somewhat overestimated values. Note that combustion between the copper cooling blocks could be terminated only when the reactive foil thickness was reduced to 20–30 μm .^{79,81} Thus, only the assumption that nickel is directly dissolved in the aluminium-based melt provides an estimate for the critical foil thickness that is in good agreement with the experimental results. The role of exothermic dissolution of nickel in liquid aluminium as a key stage of material bonding was also confirmed using MDS.¹⁴⁸

The mathematical model of combustion of a reactive layer sandwiched between semiconductor surface-oxidized silicon wafers was developed for Pd/Al RMNF.¹⁴⁹ The results of calculations demonstrated that the foil thickness can be decreased to 1.6 μm (16 bilayers, 100 nm-thick each), and this result was confirmed in experiments. The effect of the initial temperature and convective heat exchange on the combustion of Ni/Al RMNF was studied theoretically and experimentally.¹⁵⁰ It was shown that the convective cooling has a minor influence on the reaction, *i.e.*, foils react in liquids in the same way as in air. In view of the data presented in this Section, this result is quite predictable.

6. Industrial production and applications of reactive nanofilms

The main application of the reactive foils commercially manufactured exclusively under the brand name NanoFoil® is to join a wide variety of materials and products for the semiconductor industry, aerospace technology, automotive industry, electronics, biomedical and other applications. In addition, applications such as reaction initiators or retardants and electrical fuses have also been claimed. These foils have an equimolar chemical composition (Ni/Al) and two rated thicknesses, 40 and 60 μm . The propagation velocity of the reaction wave in these foils is 6.5–8.0 m s^{-1} and the heat of the reaction is 1.050–1.250 J g^{-1} (*i.e.*, 90–107 kJ mol^{-1} , or 76–91% of the enthalpy of the reaction $\text{Ni} + \text{Al} = \text{NiAl}$). The stated foil density (5.6–6.0 g cm^{-3}) exceeds the theoretical density of the initial multilayer foil (5.165 g cm^{-3}), but corresponds to the density of the reaction product — NiAl (5.9 g cm^{-3}). The thermal conductivity of the industrial foils is 35–50 $\text{W m}^{-1} \text{K}^{-1}$, which is markedly lower than the theoretical thermal conductivity of the multilayer film (120.4 $\text{W m}^{-1} \text{K}^{-1}$) and somewhat lower than the thermal conductivity of NiAl (76 $\text{W m}^{-1} \text{K}^{-1}$).¹⁵¹ The density and thermal conductivity differences are probably attributable to the presence of a solder layer on the foil surface.

A high strength of bonding between a material and RMNF can be attained if a 1–10 μm solder layer has been applied on

the foil surface, or on the surface of the material meant for joining, or on both surfaces. The solder composition is chosen depending on the practical task, ranging from simple tin–lead solder to more complex compositions such as SnAgSb, which provides high shear strengths of the joint of about 65 MPa. Gold or silver coating of the surfaces is also used. In some cases, soldering is assisted by ultrasonic treatment to increase the bonding strength.

A relevant practical task that can be solved using RMNFs is joining of parts of a large area or complex shape. Reactive Ni/Al foils shaped as rectangles with dimensions up to 106.7 \times 55.9 cm and rings up to 55.9 cm in diameter are available in the market. A technique for laser cutting of reactive foils to a desired shape has been developed.²² An infrared laser beam with approximately 1000 nm wavelength and 5–15 W power repeatedly passes along a specified line and cuts off a thin layer of the material per pass. This makes it possible to cut foil or to apply specified patterns on the foil surface without initiating the reaction. The minimum size of RMNFs present in the market is 1 \times 1 mm.

Both commercially available RMNFs and those manufactured by researchers themselves are used to solve particular practical tasks. One of the most popular applications is soldering of targets for magnetron sputtering to a heat sink, with the targets being either metallic or ceramic (Fig. 9). The second most popular application is joining of microelectronic components, *e.g.*, attaching a circuit board to a heat sink or joining of semiconductor silicon wafers.^{152,153} In many microelectronic applications, the attachment of so-called low temperature co-fired ceramics to a metallic heat sink is required. This problem was also solved using Ni/Al RMNFs.¹⁵⁴

Many applied tasks require good heat transfer between the bonded materials. Studies of the thermal resistance of the contact demonstrated the advantages of reactive Ni/Al foils over reactive layers deposited directly on the bonded surface.¹⁵⁵ Bonding of copper foils in a multilayer assembly using commercial reactive nanofilms made it possible to improve characteristics of lithium cells.¹⁵⁶ A method for bonding piezoceramics to various materials has been proposed.¹⁵⁷

Thus, bonding of materials is the predominant practical application of RMNFs. There are still little data concerning other applications, probably, since they are less developed.

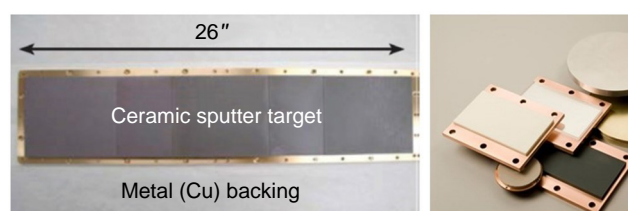


Figure 9. Targets for magnetron sputter deposition bonded to a heat sink base using RMNFs (from public source <https://www.indium.com/products/nanofoil/>).

Mention should be made of the use of Ni/Al RMNFs as foils that explode under the action of an electric current pulse, which can be used for the design of reliable small-volume initiators.¹⁵⁸ It can be expected that the range of practical applications of RMNFs will continue to expand in the coming years.

7. Conclusion

The studies of reactive multilayer nanofilms have been carried out for more than 25 years starting from the appearance of the first patent¹ for these unusual energetic materials with unique properties. Over the last 15 years covered in the present review, an impressive progress was made in experimental studies of the mechanisms of self-propagating chemical reactions in layered nanosystems. The development of the dynamic transmission electron microscopy technique, the use of synchrotron diffraction and quenching of the combustion wave resulted in determination of the dynamics of chemical, phase and microstructural transformations with a microsecond and even nanosecond resolution. In the theoretical studies of these processes, the focus is being shifted from the layer mathematical model based on the solution of a system of differential equations and extrapolated to the nano-scale to the molecular-dynamic simulation, which makes it possible to predict the real microstructure and crystal structure of the reaction products. These two approaches are mutually complementary: the information on the mass transfer mechanisms on a nanoscale gained using MDS can serve to reliably determine diffusion coefficients, which can be used in the layer models in order to calculate the macroscopic RMNF combustion modes. The beginning of the commercial manufacture and marketing of reactive nanofoils entailed the development of modern technologies for bonding dissimilar materials in the magnetron sputtering targets, microelectronic and aerospace engineering devices, and other practically important industries.

Simultaneously, fundamental studies aimed at the search for new chemical compositions in nanofoils and elucidation of the regularities and mechanisms of exothermic reactions in nanofoils are in progress. In our opinion, a promising trend is to develop chemical compositions of RMNFs that would combine the advantages of bimetallic and thermite compositions, that is, smooth combustion regime and high heat of the reaction. Perhaps, these compositions may be represented by Ti/C, Ta/C and Ti/B films and other similar films based on refractory elements. They release 1.5–2 times more heat when burn than intermetallic systems, with the combustion temperature being as high as 3000 K or even higher. In addition, evaporation of refractory reactants and products in these systems is negligibly low; hence, the reaction proceeds in a smooth gasless regime, unlike the vigorous burning of thermite compositions. A challenge associated with the design of these RMNFs is related to their unsatisfactory mechanical properties: the presence of brittle carbon and boron layers precludes the fabrication of flexible films separated from the substrate. One may hope that this problem would be solved, for example, by introduction of multilayer graphene or borophene layers into RMNFs.

The possibility of purely solid-phase propagation of exothermic reaction waves in RMNFs is still an open question. As shown in the review, combustion in any of the reactive films is accompanied by melting of at least one of the reactants. Meanwhile, the reaction is initiated at temperatures much below the melting point. The role of solid-phase reactions in the ignition was confirmed by high-speed thermography;¹⁵⁹ the

possibility of the solid-phase combustion mode (so-called ‘solid flame’) in submicrometre and nano-heterogeneous systems has been discussed.¹⁶⁰ Is it possible to design RMNF in which the self-propagating exothermic reaction would proceed without melting of any reactant or product? A positive answer to this question could open up new opportunities for the use of RMNFs, for example, in microelectronic components.

All the foregoing provides the conclusion that research and development in the field of reactive multilayer nanofoils entered the period of scientific and technological maturity. Indeed, for some RMNFs compositions (Ni/Al), the main scientific problems have been solved, their commercial manufacturing is going on, and the range of applications for solving engineering and technological problems is being expanded. Simultaneously, understanding of the fundamental combustion mechanisms of nanolayered systems becomes more profound, and promising RMNFs of new chemical compositions and microstructures have emerged on the horizon; their manufacture and applications are to be developed in the future.

8. List of abbreviations and symbols

DTEM — dynamic transmission electron microscopy;
MDS — molecular dynamic simulation;
RMNF — reactive multilayer nanofilm;
RMF — reactive multilayer foil (films separated from the substrate);
SHS — self-propagating high-temperature synthesis;
SiG (Si grass) — special microstructure of a silicon wafer (silicon grass);
 D — diffusion coefficient;
 D_0 — pre-exponential factor;
 E_a — activation energy for diffusion;
 R — gas constant;
 T — temperature.

9. References

1. Patent US 5538795 (1996)
2. A.S.Rogachev. *Russ. Chem. Rev.*, **77**, 21 (2008); <https://doi.org/10.1070/RC2008v077n01ABEH003748>
3. E.L.Dreizin. *Prog. Energy Combust. Sci.*, **35**, 141 (2009); <https://doi.org/10.1016/j.pecs.2008.09.001>
4. D.P.Adams. *Thin Solid Films*, **576**, 98 (2015); <https://doi.org/10.1016/j.tsf.2014.09.042>
5. D.Sundaram, V.Yang, R.A.Yetter. *Prog. Energy Combust. Sci.*, **61**, 293 (2017); <https://doi.org/10.1016/j.pecs.2017.02.002>
6. E.L.Dreizin, M.Schoenitz. *J. Mater. Sci.*, **52**, 11789 (2017); <https://doi.org/10.1007/s10853-017-0912-1>
7. F.Baras, V.Turlo, O.Politano, S.G.Vadchenko, A.S.Rogachev, A.S.Mukasyan. *Adv. Eng. Mater.*, **20**, 1800091 (2018); <https://doi.org/10.1002/adem.201800091>
8. S.Q.Arlington, G.M.Fritz, T.P.Weih. *Annu. Rev. Mater. Res.*, **52**, 219 (2022); <https://doi.org/10.1146/annurev-matsci-081720-124041>
9. A.S.Rogachev, A.S.Mukasyan. *Combustion for Material Synthesis*. (CRC Press, 2015). 397 p.
10. T.P.Weih. In *Metallic Films for Electronic, Optical and Magnetic Applications: Structure, Processing and Properties*. (Ed. K.Barmak, K.Coffey). (Oxford, UK: Woodhead Publ., 2014). P. 160; <https://doi.org/10.1533/9780857096296.1.160>
11. N.A.Manesh. *Heat Transfer in Multi-layer Energetic Nanofilm on Composites Substrate*. Doctoral Dissertation, University of Central Florida, 2010, 149 pp.
12. M.D.Grapes. *The Role of Interfacial Reactions in Aluminum/Nickel Reactive Multilayer Performance*. A Dissertation Submitted to Johns Hopkins University in Conformity with the Requirements for the Degree of Doctor of Philosophy, Baltimore, Maryland, 2016, 205 pp.

13. M.P.Kremer. *Development of a Bonding Concept for MOEMS Packaging: Reactive Nanocomposites*. Zur Erlangung des akademischen Grades eines Doktors der Ingenieurwissenschaften (Dr.-Ing.) bei der KIT-Fakultät für Maschinenbau des Karlsruher Instituts für Technologie (KIT) Dissertation, 2018, 187 pp.
14. S.Danzi. *From Reactive Multilayers to Healing of Metal Thin Films: Harvesting the Potential of Self-Sustained Heat Waves*. A Thesis Submitted to Attain the Degree of Doctor of Sciences of ETH Zurich, 2020, 158 pp. <https://doi.org/10.3929/ethz-b-000450195>
15. S.Sen. *Development of PVD-coated and Nanostructured Reactive Multilayer Films*. (Universitätsverlag Ilmenau, 2018), 166 pp.
16. M.Kokonou, C.Rebholz, K.P.Giannakopoulos, C.C.Doumanidis. *Nanotechnology*, **18**, 495604 (2007); <https://doi.org/10.1088/0957-4484/18/49/495604>
17. M.Kokonou, K.P.Giannakopoulos, I.E.Gunduz, K.Fadenberger, C.Rebholz, C.C.Doumanidis. *Microelectron. Eng.*, **86**, 836 (2009); <https://doi.org/10.1016/j.mee.2008.12.089>
18. C.Rebholz, I.E.Gunduz, T.Ando, C.C.Doumanidis. *Mater. Res. Express*, **2**, 045009 (2015); <https://doi.org/10.1088/2053-1591/2/4/045009>
19. M.Petrantoni, A.Hemeryck, J.M.Duc  r  , A.Est  ve, C.Rossi, M.Djafari Rouhani, D.Est  ve, G.Landa. *J. Vac. Sci. Technol. A*, **28** (6), L15 (2010); <https://doi.org/10.1116/1.3491182>
20. A.Hemeryck, M.Petrantoni, A.Est  ve, C.Rossi, M.Djafari Rouhani, G.Landa, D.Est  ve. *J. Phys. Chem. Solid.*, **71**, 125 (2010); <https://doi.org/10.1016/j.jpcc.2009.07.019>
21. B.Liu, X.Yu, Y.Qiao, L.You, Y.Wang, F.Ye. *Appl. Surface Sci.*, **546**, 149098 (2021); <https://doi.org/10.1016/j.apsusc.2021.149098>
22. M.A.Martins, D.W.M  ller, J.Schmauch, M.Glaser, J.P.Bergmann, F.M  cklich, C.Pauly. *Appl. Sci.*, **13**, 4313 (2023); <https://doi.org/10.3390/app13074313>
23. G.M.Fritz, H.Joess, T.P.Weih. *Combust. Flame*, **158**, 1084 (2010); <https://doi.org/10.1016/j.combustflame.2010.10.008>
24. A.S.Rogachev. *Russ. Chem. Rev.*, **88**, 875 (2019); <https://doi.org/10.1070/RCR4884>
25. I.E.Gunduz, A.Kyriakou, N.Vlachos, T.Kyratsi, C.C.Doumanidis, S.Son, C.Rebholz. *Surf. Coat. Technol.*, **260**, 396 (2014); <https://doi.org/10.1016/j.surfcoat.2014.06.068>
26. M.P.Kremer, A.Roshanghias, A.Tortschanoff. *Micro and Nano Syst. Lett.*, **5**, 12 (2017); <https://doi.org/10.1186/s40486-017-0046-x>
27. M.Wang, L.Qiu, X.Zhao, Y.Li, T.Rao, S.He, L.Qin, J.Tao. *Mater. Sci. Eng.: A*, **757**, 23 (2019); <https://doi.org/10.1016/j.msea.2019.04.068>
28. S.Hertel, K.Vogel, M.Wiemer, T.Otto. In *2020 IEEE 8th Electronics System-Integration Technology Conference (ESTC), T  nsberg, Norway*. (Piscataway, NJ: IEEE, 2020). P. 355; <https://doi.org/10.1109/ESTC48849.2020.9229651>
29. S.Hertel, W.Schulte, M.Weiser, M.Becker, M.Wiemer, T.Otto. In *GMM-Fachbericht 92: Mikro-Nano-Integration*. (VDE Verlag GmLH, 2018). P. 38
30. S.Q.Arlington, S.V.Lakshman, S.C.Barron, J.B.DeLisio, J.C.Rodriguez, S.Narayanan, G.M.Fritz, T.P.Weih. *Mater. Adv.*, **1**, 1151 (2020); <https://doi.org/10.1039/D0MA00148A>
31. Patent US 10240058 B2 (2019)
32. H.Bartsch, J.M.M  nuel, R.Grieseler. *Technologies*, **5**, 79 (2017); <https://doi.org/10.3390/technologies5040079>
33. Y.H.Sauni Camposano, S.S.Riegler, K.Jaekel, J.Schmauch, C.Pauly, C.Sch  fer, H.Bartsch, F.M  cklich, I.Gallino, P.Schaaf. *Appl. Sci.*, **11**, 9304 (2021); <https://doi.org/10.3390/app11199304>
34. Y.H.Sauni Camposano, H.Bartsch, S.Matthes, M.Oliva-Ramirez, K.Jaekel, P.Schaaf. *Phys. Status Solidi A*, **220**, 2200765 (2023); <https://doi.org/10.1002/pssa.202200765>
35. K.Jaekel, Y.H.Sauni Camposano, S.Matthes, M.Glaser, P.Schaaf, J.P.Bergmann, J.Muller, H.Bartsch. *J. Mater. Sci.*, **58**, 12811 (2023); <https://doi.org/10.1007/s10853-023-08794-9>
36. F.Baras, O.Politano. *Acta Mater.*, **148**, 133 (2018); <https://doi.org/10.1016/j.actamat.2018.01.035>
37. S.Danzi, M.Men  trety, J.Wohlwend, R.Spolenak. *ACS Appl. Mater. Interfaces*, **11**, 45 (2019); <https://doi.org/10.1021/acsami.9b14660>
38. I.A.Korz. *Tekhn. Radiosvyazi*, **2** (45), 71 (2020); <https://doi.org/10.33286/2075-8693-2020-45-71-79>
39. I.A.Korz. *Tekhn. Radiosvyazi*, **3** (54), 93 (2022);
40. A.E.Grigoryan, N.G.Elistratov, D.Yu.Kovalev, A.G.Merzhanov, A.N.Nosyrev, V.I.Ponomarev, A.S.Rogachev, V.I.Khvesyuk, P.A.Tsygankov. *Dokl. Phys. Chem.*, **381**, 283 (2001); <https://doi.org/10.1023/A:1012952211911>
41. M.J.Abere, G.C.Egan, D.E.Kittell, G.H.Campbell, D.P.Adams. *AIP Adv.*, **10**, 085012 (2020); <https://doi.org/10.1063/5.0015317>
42. K.R.Overdeep, H.Joess, L.Zhou, K.J.T.Livi, S.C.Barron, M.D.Grapes, K.S.Shanks, D.S.Dale, M.W.Tate, H.T.Philipp, S.M.Gruner, T.C.Hufnagel, T.P.Weih. *Combust. Flame*, **191**, 442 (2018); <https://doi.org/10.1016/j.combustflame.2017.11.023>
43. C.D.Yarrington, M.J.Abere, D.P.Adams, M.L.Hobbs. *J. Appl. Phys.*, **121**, 134301 (2017); <http://dx.doi.org/10.1063/1.4979578>
44. M.J.Abere, C.D.Yarrington, D.P.Adams. *J. Appl. Phys.*, **123**, 235304 (2018); <https://doi.org/10.1063/1.5026507>
45. M.J.Abere, C.D.Yarrington, P.G.Kotula, J.P.McDonald, D.P.Adams. *J. Phys. Chem. C*, **125**, 9756 (2021); <https://doi.org/10.1021/acs.jpcc.1c01776>
46. D.P.Adams, M.J.Abere, C.Sobczak, M.A.Rodriguez. *Thin Solid Films*, **688**, 137349 (2019); <https://doi.org/10.1016/j.tsf.2019.05.068>
47. J.-C.Gachon, A.S.Rogachev, H.E.Grigoryan, E.V.Illarionova, J.-J.Kuntz, D.Yu.Kovalev, A.N.Nosyrev, N.V.Sachkova, P.A.Tsygankov. *Acta Mater.*, **53**, 1225 (2005); <https://doi.org/10.1016/j.actamat.2004.11.016>
48. H.Joess, S.C.Barron, K.J.T.Livi, N.Aronhime, T.P.Weih. *Appl. Phys. Lett.*, **101** (11), 111908 (2012); <https://doi.org/10.1063/1.4752133>
49. M.Vohra, T.P.Weih. *Combust. Flame*, **162**, 249 (2014); <https://doi.org/10.1016/j.combustflame.2014.07.010>
50. E.-M.Bourim, I.-S.Kang, H.Y.Kim. *Micromachines*, **12**, 1272 (2021); <https://doi.org/10.3390/mi12101272>
51. K.Woll, I.E.Gunduz, C.Pauly, C.C.Doumanidis, S.F.Son, C.Rebholz, F.Muecklich. *Appl. Phys. Lett.*, **107**, 073103 (2015); <https://doi.org/10.1063/1.4928665>
52. K.Woll, A.Bergamaschi, K.Avchachov, F.Djurabekova, S.Gier, C.Pauly, P.Leibenguth, C.Wagner, K.Nordlund, F.Muecklich. *Sci. Rep.*, **6**, 19535 (2016); <https://doi.org/10.1038/srep19535>
53. C.Pauly, K.Woll, B.Bax, F.Muecklich. *Appl. Phys. Lett.*, **107**, 113104 (2015); <https://doi.org/10.1063/1.4930022>
54. D.P.Adams, M.A.Rodriguez, J.P.McDonald, M.M.Bai, E.Jones Jr., L.Brewer, J.J.Moore. *J. Appl. Phys.*, **106**, 093505 (2009); <https://doi.org/10.1063/1.3253591>
55. B.Boettge, J.Brauer, M.Wiemer, M.Petzold, J.Bagdahn, T.Gessner. *J. Micromech. Microeng.*, **20**, 064018 (2010); <https://doi.org/10.1088/0960-1317/20/6/064018>
56. Y.Kuntani, D.Goto, K.Maekawa, K.Kodama, S.Kanetsuki, S.Miyake, T.Namazu. *Jpn. J. Appl. Phys.*, **59** (2020); <https://doi.org/10.35848/1347-4065/ab827f>
57. S.M.Zharkov, R.R.Altunin, E.T.Moiseenko, G.M.Zeer, S.N.Varnakov, S.G.Ovchinnikov. *Solid State Phenomena*, **215**, 144 (2014); <https://doi.org/10.4028/www.scientific.net/SSP.215.144>
58. S.Sen, M.Lake, R.Grieseler, P.Schaaf. *Surf. Coat. Technol.*, **327**, 25 (2017); <https://doi.org/10.1016/j.surfcoat.2017.07.065>
59. M.E.Reiss, C.M.Esber, D.Van Heerden, A.J.Gavens, M.E.Williams, T.P.Weih. *Mater. Sci. Eng., A*, **261**, 217 (1999); [https://doi.org/10.1016/S0921-5093\(98\)01069-7](https://doi.org/10.1016/S0921-5093(98)01069-7)
60. L.A.Clevenger, C.V.Tompson, K.N.Tu. *J. Appl. Phys.*, **67**, 2894 (1990); <https://doi.org/10.1063/1.345429>

61. S.Q.Arlington, T.Neuhauser, M.Short, K.Woll, D.A.LaVan, G.M.Fritz, T.P.Weih. *Mater. Design*, **225**, 111514 (2023); <https://doi.org/10.1016/j.matdes.2022.111514>
62. K.J.Blobaum, M.E.Reiss, J.M.Plitzko, T.P.Weih. *J. Appl. Phys.*, **94**, 2915 (2003); <https://doi.org/10.1063/1.1598296>
63. K.J.Blobaum, A.J.Wagner, J.M.Plitzko, D.Van Heerden, D.H.Fairbrother, T.P.Weih. *J. Appl. Phys.*, **94**, 2923 (2003); <https://doi.org/10.1063/1.1598297>
64. C.Rossi. *Propellants Explos. Pyrotech.*, **44**, 94 (2019); <https://doi.org/10.1002/prep.201800045>
65. W.Guo, S.Chang, J.Cao, L.Wu, R.Shen, Y.Ye. *Nanoscale Res. Lett.*, **14**, 301(2019); <https://doi.org/10.1186/s11671-019-3124-6>
66. L.Salvagnac, S.Assie-Souleille, and C.Rossi. *Nanomaterials*, **10**, 2009 (2020); <https://doi.org/10.3390/nano10102009>
67. Y.Shen, J.Xu, C.Wang, T.Yang, Y.Ye, R.Shen. *Sens. Actuators*, **A313**, 112200 (2020); <https://doi.org/10.1016/j.sna.2020.112200>
68. C.Rossi, K.Zhang, D.Esteve, P.Alphonse, P.Tailhades, C.Vahlas. *J. Microelectromech. Syst.*, **16(4)**, 919 (2007); <https://doi.org/10.1109/JMEMS.2007.893519>
69. C.Rossi, A.Este've, P.Vashishta. *J. Phys. Chem. Solids*, **71** (2), 57 (2010); <https://doi.org/10.1016/j.jpcs.2009.10.015>
70. S.B.Kim, K.J.Kim, M.H.Cho, J.H.Kim, K.T.Kim, S.H.Kim. *ACS Appl. Mater. Interfaces*, **8** (14), 9405 (2016); <https://doi.org/10.1021/acsami.6b00070>
71. S.S.Pandey, N.Banerjee, Y.Xie, C.H.Maistrangelo. *Adv. Mater. Technol.*, **3**, 1800044 (2018); <https://doi.org/10.1002/admt.201800044>
72. A.Nicollet, L.Salvagnac, V.Baijot, A.Esteve, C.Rossi. *Sens. Actuators*, **A 273**, 249 (2018); <https://doi.org/10.1016/j.sna.2018.02.044>
73. A.H.Kinsey, K.Slusarski, K.Woll, D.Gibbins, T.P.Weih. *J. Mater. Sci.*, **51(12)**, 5738 (2016); <https://doi.org/10.1007/s10853-016-9876-9>
74. M.Wiemer, C.Hofmann, K.Vogel. *ECS Trans.*, **98** (4), 183 (2020); <https://doi.org/10.1149/09804.0183ecst>
75. A.H.Kinsey, K.Slusarski, S.Sosa, T.P.Weih. *ACS Appl. Mater. Interfaces*, **9** (26), 22026 (2017); <http://dx.doi.org/10.1021/acsami.7b17709>
76. A.H.Kinsey, R.Behrou, J.K.Guest, T.P.Weih. *Combust. Flame*, **190**, 432 (2018); <https://doi.org/10.1016/j.combustflame.2017.12.017>
77. A.Nicollet, G.Lahiner, A.Belisario, S.Souleille, M.Djafari-Rouhani, A.Estève, C.Rossi. *J. Appl. Phys.*, **121**, 034503 (2017); <http://dx.doi.org/10.1063/1.4974288>
78. V.G.Myagkov. *arXiv*:1903.11784 (2019); <https://doi.org/10.48550/arXiv.1903.11784>
79. A.S.Rogachev, S.G.Vadchenko, A.S.Mukasyan. *Appl. Phys. Lett.*, **101**, 063119 (2012); <https://doi.org/10.1063/1.4745201>
80. A.S.Rogachev, S.G.Vadchenko, F.Baras, O.Politano, S.Rouvimov, N.V.Sachkova, A.S.Mukasyan. *Acta Mater.*, **66**, 86 (2014); <https://doi.org/10.1016/j.actamat.2013.11.045>
81. A.S.Rogachev, S.G.Vadchenko, F.Baras, O.Politano, S.Rouvimov, N.V.Sachkova, M.D.Grapes, T.P.Weih, A.S.Mukasyan. *Combust. Flame*, **166**, 158 (2016); <https://doi.org/10.1016/j.combustflame.2016.01.014>
82. C.Michaelsen, G.Lucadamo, K.Barmak. *J. Appl. Phys.*, **80**, 6689 (1996); <https://doi.org/10.1063/1.363794>
83. E.A.Lebedev, A.S.Rogachev, S.G.Vadchenko, D.G.Gromov, M.I.Alymov. *Appl. Phys. Lett.*, **121**, 1319023 (2022); <https://doi.org/10.1063/5.0109018>
84. A.I.Novoseltsev, L.I.Sorokina, A.V.Sysa, R.M.Ryazanov, E.A.Lebedev. *J. Phys.: Conf. Ser.*, **2086**, 012213 (2021); <https://doi.org/10.1088/1742-6596/2086/1/012213>
85. M.E.Shiryaev, A.I.Novosel'tsev, R.M.Ryazanov, A.V.Sysa, E.A.Lebedev. *Issledovanie Vliyaniya Tolshchiny Mnogosloynnykh Termitnykh Struktur Al–CuO na Kharakteristiki Produktov Reaktsii Roreniya. In Materialy Nauchno-Tekhnicheskoi Konferentsii. (Study of the Influence of the Thickness of Multilayer Thermite Structures Al–CuO on the Characteristics of Combustion Reaction Products. In Materials of the Scientific and Technical Conference)*. (Moscow, 2023). P. 296; <https://www.miet.ru/page/149658>
86. J.Kim, T.LaGrande, B.Reed, M.Taheri, M.Armstrong, W.King, N.Browning, G.Campbell. *Science*, **321** (5895), 1472 (2008); <https://doi.org/10.1126/science.1161517>
87. T.LaGrande, G.H.Campbell, B.W.Reed, M.Taheri, J.B.Pesavento, J.S.Kim, N.D.Browning. *Ultramicroscopy*, **108**, 1441 (2008); <https://doi.org/10.1016/j.ultramic.2008.03.013>
88. G.Campbell, T.LaGrande, J.Kim, B.Reed, N.Browning. *J. Electron Microscopy*, **59** (Suppl.), 567 (2010); <https://doi.org/10.1093/jmicro/dfq032>
89. J.Kim, T.LaGrande, B.Reed, R.Knepper, T.Weih, N.Browning, G.Campbell. *Acta Mater.*, **59** (9), 3571 (2011); <https://doi.org/10.1016/j.actamat.2011.02.030>
90. M.Picher, S.Sinha, T.LaGrange, F.Banhart. *ChemTexts*, **8**, 18 (2022); <https://doi.org/10.1007/s40828-022-00169-y>
91. M.Picher, S.Sinha, Y.Hu, T.LaGrange, F.Banhart. *Micros. Microanal.*, **28**, 1790 (2022); <https://doi.org/10.1017/S1431927622007073>
92. M.D.Grapes, T.LaGrande, L.H.Friedman, B.W.Reed, G.H.Campbell, T.P.Weih. *Rev. Sci. Instrum.*, **85**, 084902 (2014); <https://doi.org/10.1063/1.4892537>
93. F.M.Alcorn, P.K.Jain, R.M.van der Veen. *Nat. Rev. Chem.*, **7** (4), 256 (2023); <https://doi.org/10.1038/s41570-023-00469-y>
94. R.R.Altunin, E.T.Moiseenko, S.M.Zharkov. *Phys. Solid State*, **62** (1), 200 (2020); <https://doi.org/10.1134/S1063783420010059>
95. E.T.Moiseenko, R.R.Altunin, S.M.Zharkov. *Metall. Mater. Trans. A* **51**, 1428–1436 (2020); <https://doi.org/10.1007/s11661-019-05602-5>
96. E.T.Moiseenko, S.M.Zharkov, R.R.Altunin, O.V.Belousov, L.A.Solovyov, V.V.Yumashev, M.N.Volochaev, G.M.Zeer. *JOM*, **73**, 580 (2021); <https://doi.org/10.1007/s11837-020-04522-9>
97. E.T.Moiseenko, V.V.Yumashev, R.R.Altunin, L.A.Solovyov, M.N.Volochaev, O.V.Belousov, S.M.Zharkov. *Materialia*, **28**, 101747 (2023); <https://doi.org/10.1016/j.mtla.2023.101747>
98. R.R.Altunin, E.T.Moiseenko, S.M.Zharkov. *Phys. Solid State*, **60** (7), 1413 (2018); <https://doi.org/10.1134/S106378341807003X>
99. V.G.Myagkov, L.E.Bykova, V.S.Zhigalov, A.A.Matsynin, D.A.Velikanov, G.N.Bondarenko. *J. Alloys Compd.*, **706**, 447 (2017); <https://doi.org/10.1016/j.jallcom.2017.02.261>
100. V.G.Myagkov, L.E.Bykova, V.S.Zhigalov, A.A.Matsynin, D.A.Velikanov, G.N.Bondarenko. *J. Alloys Compd.*, **849**, 157938 (2020); <https://doi.org/10.1016/j.jallcom.2020.157938>
101. S.M.Zharkov, E.T.Moiseenko, R.R.Altunin, N.S.Nikolaeva, V.S.Zhigalov, V.G.Myagkov. *JETP Lett.*, **99** (7), 405 (2014); <https://doi.org/10.1134/S0021364014070145>
102. S.M.Zharkov, E.T.Moiseenko, R.R.Altunin. *J. Solid State Chem.*, **269**, 36 (2019); <https://doi.org/10.1016/j.jssc.2018.09.009>
103. V.G.Myagkov, A.A.Ivanenko, L.E.Bykova, V.S.Zhigalov, M.N.Volochaev, D.A.Velikanov, A.A.Matsynin, G.N.Bondarenko. *Sci. Rep.*, **10**, 10807 (2020); <https://doi.org/10.1038/s41598-020-67837-2>
104. V.G.Myagkov, L.E.Bykova, V.S.Zhigalov, A.A.Matsynin, S.M.Zharkov, A.A.Ivanenko, G.N.Bondarenko, D.A.Velikanov. *Intermetallics*, **157**, 107871 (2023); <https://doi.org/10.1016/j.intermet.2023.107871>
105. L.E.Bykova, S.M.Zharkov, V.G.Myagkov, Yu.Yu.Balashov, G.S.Patrin. *Phys. Solid State*, **64**, 33 (2022); <https://doi.org/10.1134/S1063783422010048>
106. S.M.Zharkov, R.R.Altunin, V.V.Yumashev, E.T.Moiseenko, O.V.Belousov, L.A.Solovyov, M.N.Volochaev, G.M.Zeer. *J. Alloys Compd.*, **871**, 159474 (2021); <https://doi.org/10.1016/j.jallcom.2021.159474>
107. E.T.Moiseenko, V.V.Yumashev, R.R.Altunin, G.M.Zeer, N.S.Nikolaeva, O.V.Belousov, S.M.Zharkov. *Materials*, **15**, 8457 (2022); <https://doi.org/10.3390/ma15238457>
108. S.M.Zharkov, V.V.Yumashev, E.T.Moiseenko, R.R.Altunin, L.A.Solovyov, M.N.Volochaev, G.M.Zeer, N.S.Nikolaeva,

- O.V.Belousov. *Nanomaterials*, **13**, 2925 (2023); <https://doi.org/10.3390/nano13222925>
109. L.E.Bykova, S.M.Zharkov, V.G.Myagkov, V.S.Zhigalov, G.S.Patrin. *JOM*, **72**, 2139 (2020); <https://doi.org/10.1007/s11837-019-03919-5>
110. V.G.Myagkov, V.S.Zhigalov, L.E.Bykova, S.M.Zharkov, A.A.Matsynin, M.N.Volochaev, I.A.Tambasov, G.N.Bondarenko. *J. Alloys Compd.*, **665**, 197 (2016); <https://doi.org/10.1016/j.jallcom.2015.12.257>
111. V.G.Myagkov, L.E.Bykova, O.A.Bayukov, V.S.Zhigalov, I.A.Tambasov, S.M.Zharkov, A.A.Matsynin, G.N.Bondarenko. *J. Alloys Compd.*, **636**, 223 (2015); <https://doi.org/10.1016/j.jallcom.2015.02.012>
112. J.C.Trenkle, L.J.Koerner, M.W.Tate, S.M.Gruner, T.P.Weih, T.C.Hufnagel. *Appl. Phys. Lett.*, **93**, 081903 (2008); <https://doi.org/10.1063/1.2975830>
113. K.Fadenberger, I.E.Gunduz, C.Tsotsos, M.Kokonou, S.Gravani, S.Brandstetter, A.Bergamaschi, B.Schmitt, P.H.Mayrhofer, C.C.Doumanidis, C.Rebholz. *Appl. Phys. Lett.*, **97**, 144101 (2010); <https://doi.org/10.1063/1.3485673>
114. S.Ramachandran, Y.Zhong, S.Robertson, C.Panteli, S.Liang, F.Wu, R.Zhou, S.Marathe, Z.Zhou, A.S.Holmes, S.J.Haigh, C.Liu, W.Mirihanage. *Materialia*, **23**, 101444 (2022); <https://doi.org/10.1016/j.mtla.2022.101444>
115. A.S.Mukasyan, A.S.Rogachev. *Progress Energy Combustion Sci.*, **34**, 377 (2008); <https://doi.org/10.1016/j.peccs.2007.09.002>
116. E.Besnoin, S.Cerutti, O.M.Knio, T.P.Weih. *J. Appl. Phys.*, **92**, 5474 (2002); <https://doi.org/10.1063/1.1509840>
117. K.Kim. *Korean J. Met. Mater.*, **57(2)**, 97 (2019); <https://doi.org/10.3365/KJMM.2019.57.2.97>
118. T.Ejima, T.Yamamura, N.Uchida, Y.Matsuzaki, M.Nikaido. *J. Jpn. Inst. Met.*, **44**, 316 (1980); https://doi.org/10.2320/jinstmet1952.44.3_316
119. A.Meyer, S.Stuber, D.Holland-Moritz, O.Heinen, T.Unruh. *Phys. Rev. B*, **77**, 092201 (2008); <https://doi.org/10.1103/PhysRevB.77.092201>
120. S.Stuber, D.Holland-Moritz, T.Unruh, A.Meyer. *Phys. Rev. B*, **81**, 024204 (2010); <https://doi.org/10.1103/PhysRevB.81.024204>
121. M.J.Chelukara, K.G.Vishnu, A.Strachan. *Phys. Rev. B*, **86**, 075470 (2012); <https://doi.org/10.1103/PhysRevB.86.075470>
122. J.M.Pauls, C.E.Shuck, A.Genc, S.Rouvimov, A.S.Mukasyan. *J. Solid State Chem.*, **276**, 114 (2019); <https://doi.org/10.1016/j.jssc.2019.04.024>
123. J.F.Zhao, C.Unuvar, U.Anselmi-Tamburini, Z.A.Munir. *Acta Mater.*, **55**, 5592 (2007); <https://doi.org/10.1016/j.actamat.2007.06.016>
124. M.M.G.Aleman, C.Rey, L.J.Gallego. *J. Chem. Phys.*, **111**, 9111 (1999); <https://doi.org/10.1063/1.480252>
125. C.Lanthony, M.Guiltat, J.M.Duc  r  , A.Verdier, A.H  meryck, M.Djafari-Rouhani, C.Rossi, Y.J.Chabal, A.Est  ve. *ACS Appl. Mater. Interfaces*, **6**, 15086 (2014); <https://doi.org/10.1021/am503126k>
126. E.J.Mily, A.Oni, J.M.LeBeau, Y.Liu, H.J.Brown-Shaklee, J.F.Ihlefeld, J.P.Maria. *Thin Solid Films*, **562**, 405 (2014); <https://doi.org/10.1016/j.tsf.2014.05.005>
127. G.Lahiner, A.Nicollet, J.Zapata, L.Marin, N.Richard, M.Djafari-Rouhani, C.Rossi, A.Est  ve. *J. Appl. Phys.*, **122**, 155105 (2017); <https://doi.org/10.1016/j.tsf.2014.05.005>
128. S.Brotman, M.D.Rouhani, C.Rossi, A.Est  ve. *J. Appl. Phys.*, **125**, 035102 (2019); <https://doi.org/10.1063/1.5063285>
129. V.Turlo, F.Baras, O.Politano. *Modelling Simul. Mater. Sci. Eng.*, **25**, 064002 (2017); <https://doi.org/10.1088/1361-651X/aa6cfa>
130. O.Politano, F.Baras, A.Mukasyan, S.G.Vadchenko, A.S.Rogachev. *Surface Coatings Technol.*, **215**, 485 (2013); <https://doi.org/10.1016/j.surfcoat.2012.09.065>
131. P.Yi, M.L.Falk, T.P.Weih. *J. Appl. Phys.*, **124**, 165303 (2018); <https://doi.org/10.1063/1.5048911>
132. B.Witbeck, D.E.Spearot. *J. Mater. Res.*, **34**, 2229 (2019); <https://doi.org/10.1557/jmr.2019.53>
133. F.Baras, O.Politano, Y.Li, V.Turlo. *Nanomaterials*, **13**, 2134 (2023); <https://doi.org/10.3390/nano13142134>
134. F.Baras, O.Politano, A.Fourmont, S.Le Gallet, A.Nepapushev, A.Sedegov, S.Vadchenko, A.Rogachev. In *XV International Symposium on Self-Propagating High-Temperature Synthesis*. (Chernogolovka: IPCP RAS, 2019). P. 49
135. V.Turlo, O.Politano, F.Baras. *Acta Mater.*, **120**, 189 (2016); <https://doi.org/10.1016/j.actamat.2016.08.014>
136. V.Turlo, O.Politano, F.Baras. *J. Alloys Compd.*, **708**, 41089 (2017); <https://doi.org/10.1016/j.jallcom.2017.03.051>
137. V.Turlo, O.Politano, F.Baras. *J. Appl. Phys.*, **121**, 055304 (2017); <https://doi.org/10.1063/1.4975474>
138. O.Politano, A.S.Rogachev, F.Baras. *J. Mater. Eng. Perform.*, **30** (5), 3160 (2021); <https://doi.org/10.1007/s11665-021-05520-x>
139. V.Turlo, O.Politano, F.Baras. *Acta Mater.*, **99**, 363 (2015); <https://doi.org/10.1016/j.actamat.2015.07.076>
140. S.S.Rybanin, S.L.Sobolev. *Combust. Explos. Shock Waves*, **25**, 524 (1989); <https://doi.org/10.1007/BF00772962>
141. A.V.Lykov. *Teplomassoobmen (Spravochnik) [Heat and Mass Transfer (Handbook)]*. (Moscow: Energiya, 1971). P. 129
142. *Fizicheskie Velichiny: Spravochnik (Physical Quantities: Handbook)*. (Eds I.S.Grigor'ev, E.Z.Meilikhov). (Moscow: Energoatomizdat, 1991). 1232 p.
143. St.Frank, S.V.Divinski, U.Sodervall, Chr.Herzig. *Acta Mater.*, **49**, 1399 (2001); [https://doi.org/10.1016/S1359-6454\(01\)00037-4](https://doi.org/10.1016/S1359-6454(01)00037-4)
144. A.V.Evtcev, E.V.Levchenko, I.V.Belova, G.E.Murch. *Intermetallics*, **19**, 848 (2011); <https://doi.org/10.1016/j.intermet.2011.01.010>
145. E.V.Levchenko, T.Ahmed, A.V.Evtcev. *Acta Mater.*, **136**, 74 (2017); <https://doi.org/10.1016/j.actamat.2017.06.056>
146. F.Demmel, D.Szubrin, W.-C.Pilgrim, C.Morkel. *Phys. Rev. B*, **84**, 014307 (2011); <https://doi.org/10.1103/PhysRevB.84.014307>
147. F.Kargl, H.Weis, T.Unruh, A.Meyer. *J. Phys.: Conference Ser.*, **340**, 012077 (2012); <https://doi.org/10.1088/1742-6596/340/1/012077>
148. F.Baras, V.Turlo, O.Politano. *J. Mater. Eng. Perform.*, **25**, 3270 (2016); <https://doi.org/10.1007/s11665-016-1989-4>
149. R.Masser, J.Brauer, T.Gessner. *J. Appl. Phys.*, **115**, 244311 (2014); <https://doi.org/10.1063/1.4885457>
150. M.Baloochi, D.Shekhawat, S.S.Riegler, S.Matthes, M.Glaser, P.Schaaf, J.P.Bergmann, I.Gallino, J.Pezoldt. *Materials*, **14**, 7815 (2021); <https://doi.org/10.3390/ma14247815>
151. G.K.Dey. *S  dhan  *, **28**, 247 (2003); <https://doi.org/10.1353/chq.0.1513>
152. J.Matteau. In *44th International Symposium on Microelectronics*. (Long Beach, CA, 000521 (October 9-13, 2011); <https://doi.org/10.4071/isom-2011-WA2-Paper5>
153. J.Brauer, J.Besser, S.Braun, R.Masser, T.Gessner, W.Schneider. *ECS Transactions*, **64**, 329 (2014); <https://doi.org/10.1149/06405.0329ecst>
154. R.Grieseler, T.Welker, J.M  ller, P.Schaaf. *Phys. Status Solidi, A*, **209**, 512 (2012); <https://doi.org/10.1002/pssa.201127470>
155. S.Kanetsuki, S.Miyake, T.Namazu. *Sens. Mater.*, **31**, 729 (2019); <https://doi.org/10.18494/SAM.2019.2076>
156. C.Luo, Y.Zhang. *J. Mater. Proc. Technol.*, **298**, 117294 (2021); <https://doi.org/10.1016/j.jmatprotec.2021.117294>
157. Patent RU 2019000023 (2020)
158. T.Wang, Q.Zeng, M.Li. *Cent. Eur. J. Energ. Mater.*, **14** (3), 547 (2017); <https://doi.org/10.22211/cejem/75605>
159. K.Manukyan, J.Pauls, C.Shuck, S.Rouvimov, A.Mukasyan, K.Nazaretyan, H.Chatilyan, S.Kharatyan. *J. Phys. Chem. C*, **122**, 27082 (2018); <https://doi.org/10.1021/acs.jpcc.8b09075>
160. A.S.Mukasyan, C.E.Shuck, J.M.Pauls, K.V. Manukyan, D.O.Moskovskikh, A.S.Rogachev. *Adv. Eng. Mater.*, **20** (8), 1701065 (2018); <https://doi.org/10.1002/adem.201701065>